ACS APPLIED MATERIALS & INTERFACES

www.acsami.org

Research Article

Peptide-Targeted High-Density Lipoprotein Nanoparticles for Combinatorial Treatment against Metastatic Breast Cancer

Chuli Jiang, Xingyue Wang, Biyun Teng, Zhe Wang, Fenghe Li, Yu Zhao, Yuan Guo,* and Qiu Zeng*

Cite This: *ACS Appl. Mater. Interfaces* 2021, 13, 35248−35265

Read Online

ACCESS | Metrics & More | Article Recommendations | Supporting Information

ABSTRACT: The sonic hedgehog (SHH) signaling pathway exhibits aberrant activation in triple-negative breast cancer (TNBC), wherein it regulates several malignant phenotypes related to tumor metastasis. GANT61, an inhibitor of the SHH signaling pathway, may offer promise when administered in combination with conventional chemotherapy to treat metastatic TNBC. However, poor bioavailability and substantial off-target toxicity limit its clinical application. To address these limitations, we designed a peptide-functionalized dual-targeting delivery system encapsulating paclitaxel and GANT61 in tLyP-1 peptide-modified reconstituted high-density lipoprotein nanoparticle (tLyP-1-rHDL-PTX/GANT61 NP) for metastatic TNBC treatment. The apolipoprotein A-1 and tLyP-1 peptide modified on the surface of nanoparticles enable the delivery system to target tumor cells by binding to the overexpressed scavenger receptor B type I and neuropilin-1 receptor. Moreover, the tLyP-1 peptide also enables the deep tumor penetration of nanoparticles further facilitating paclitaxel and GANT61 delivery. Increased cellular uptake of the nanoparticles was observed in both MDA-MB-231, BT-549 tumor cells, and their 3D tumor spheroids. A series of *in vitro* experiments reveal that GANT61 was able to suppress key metastasis-related tumor cell activities including angiogenesis, migration, invasion, and stemness. Owing to more effective drug administration, the metastasis suppression efficiency of GANT61 was significantly enhanced by the dual-targeting tLyP-1-rHDL delivery system. Meanwhile, the codelivery of paclitaxel and GANT61 by dual-targeting tLyP-1-rHDL nanoparticles demonstrated superior efficiency of disrupting proliferation and inducing apoptosis in tumor cells compared with drug solutions. In a spontaneous metastasis breast cancer NCG mice model, the tLyP-1-rHDL-PTX/GANT61 nanoparticles exhibited highly tumor-specific distribution and result in significant inhibition of the primary tumor growth and dramatic reduction of lung metastasis without obvious side effects. The present work suggests that a combination of the SHH signaling pathway suppression and chemotherapy assisted by peptide-functionalized targeting tLyP-1-rHDL nanoparticles may provide a promising strategy for metastatic TNBC treatment.

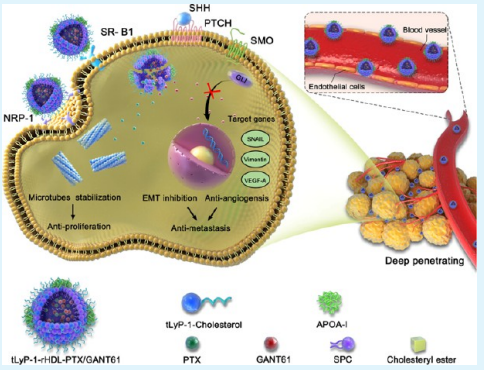

KEYWORDS: *triple-negative breast cancer, reconstituted high-density lipoprotein, cell-penetrating peptide, sonic hedgehog signaling pathway, metastasis*

1. INTRODUCTION

Breast cancer is among the deadliest cancers in the world affecting women.[1,2] Paclitaxel (PTX) is a chemotherapeutic drug used to treat breast cancer that interferes with spindle microtubules, resulting in cell cycle arrest and apoptotic death.[3] The combination of PTX and targeted antibody therapy can significantly improve the overall survival (OS) of some patients with specific breast cancer subtypes.[4] Triple-negative breast cancer (TNBC), so named for its lack of human epidermal growth factor receptor 2 (HER2), progesterone receptor, or estrogen receptor expression, is an aggressive subtype that accounts for 10−20% of overall cases.[5] Owing to a lack of well-defined tumor targets, TNBC patients generally have a poor prognosis relative to individuals with other disease subtypes.[6] TNBC is also linked to high rates of distant metastasis, leading to adverse patient outcomes.[7,8] As such, novel therapeutic targets associated with TNBC and effective treatments for such tumor metastasis must be identified to improve patient prognosis.

The sonic hedgehog (SHH) signaling pathway has previously shown to be aberrantly activated in TNBC.[9,10] Glioma-associated oncogene transcription factor 1 (GLI1) is a primary SHH signaling pathway effector molecule that controls the expression of a range of downstream target genes such as vascular endothelial growth factor A (VEGF-A), thrombospondin 1 (THBS1), snail homologue 1 (SNAIL), and Vimentin (VIM).[11−13] These genes are, in turn, responsible

Received: January 31, 2021
Accepted: July 9, 2021
Published: July 21, 2021

https://doi.org/10.1021/acsami.1c02074
ACS Appl. Mater. Interfaces 2021, 13, 35248−35265

Scheme 1. Schematic Illustration of the Structure and Antitumor Mechanisms of tLyP-1-rHDL-PTX/GANT61 NPs in the Context of TNBC Therapy[a]

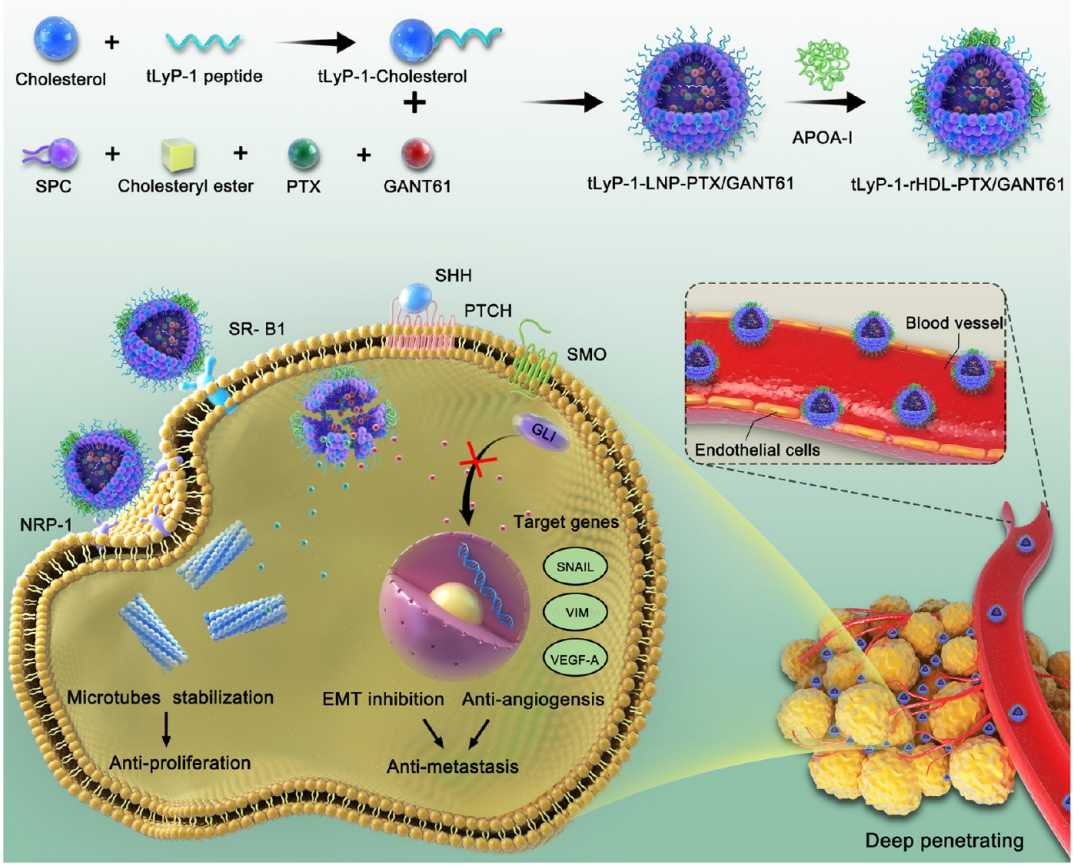

[a]Hydrophobic GANT61 and PTX were passively encapsulated into nanoparticles. Upon intravenous administration, tLyP-1-rHDL-PTX/GANT61 NPs could preferentially accumulate within tumor tissues owing to the SR-B1 and NRP-1 receptor-mediated binding. These NPs were then internalized by tumor cells whereupon PTX and GANT61 were released. PTX was capable of inhibiting the proliferation of tumor cells *via* stabilizing microtubules. Simultaneously, the SHH pathway inhibitor GANT61 regulated multiple downstream target genes and inhibited the epithelial-mesenchymal transition and angiogenesis of tumor cells by antagonizing the GLI1 transcription factor. The synergistic therapeutic effects of PTX and GANT61 resulted in the inhibition of the primary tumor growth and suppressed tumor metastasis (PTCH: protein patched homologue 1; SMO: smoothened; VEGF-A: vascular endothelial growth factor A; SNAIL: snail homologue 1; VIM: Vimentin; and EMT: epithelial−mesenchymal transition).

for driving tumor neovascularization and epithelial-to-mesenchymal transition, thus promoting metastatic progression. Inhibiting SHH pathway activation may thus represent an ideal approach to treat metastatic TNBC.

The hexahydro pyrimidine derivative GANT61 has been shown to antagonize GLI1 transcription factor activity by disrupting its processing, ciliary trafficking, or DNA binding.[14,15] As such, combination PTX and GANT61 treatment may represent an effective approach to the enhanced treatment of primary tumors and distant metastases. However, owing to its unstable structure and poor pharmacokinetic properties, achieving therapeutic intratumoral concentrations of GANT61 is often challenging, limiting its clinical application.[16] In addition, antitumor drug use can also be constrained by the severe systemic toxicity of these agents.[17] For example, PTX can cause myelosuppression, peripheral neuropathy, nausea, and diarrhea, reducing patient compliance and associated therapeutic utility.[18,19] Combination GANT61 and PTX treatment may result in even more severe adverse effects. It is thus important that new drug-delivery approaches be designed that can directly deliver drugs to tumor cells, thereby improving combinatorial drug efficacy while minimizing the incidence of such adverse events.

Targeted nanoparticle (NP)-based drug-delivery systems have been explored in recent years as increasingly promising approaches to overcome limitations associated with effective drug administration.[20−22] Herein, we propose the design of novel biodegradable NPs based on reconstituted high-density lipoprotein (rHDL) for such delivery applications. These lipid-based particles contain a hydrophilic shell and a hydrophobic core and are composed of natural compounds including phospholipids, cholesterol, cholesterol esters, and apolipoprotein A-1 (apoA-1).[23,24] Owing to their physiochemical properties, these NPs can readily encapsulate hydrophobic drugs and can effectively evade the reticuloendothelial system.[25−28] By placing apoA-1 on the surface of rHDL NPs, it is possible to enhance their ability to interact with scavenger type B1 receptor (SR-B1), which is overexpressed in TNBC cells,[29,30] thereby allowing for direct tumor targeting. Even in the context of such tumor targeting, however, the ability of NPs to penetrate tumors may be limited by the disorganized intratumoral vasculature and high interstitial pressure values.[31,32] The conjugation of specific peptides to the surface

https://doi.org/10.1021/acsami.1c02074
ACS Appl. Mater. Interfaces 2021, 13, 35248−35265

of these NPs may represent a means of overcoming such limitations.[33−35] The tLyP-1 peptide (sequence: CGNKRTR) reportedly serves as a ligand for the neuropilin-1 (NRP-1) receptor that is expressed at elevated levels on breast cancer cells.[36,37] Leveraging the tLyP-1 peptide can promote extravasation and tissue penetration *via* NRP-1-dependent C-end rule (CendR) internalization, thereby enabling the improved penetration of drug-delivery platforms into tumors.[38,39] Modifying the surfaces of rHDL particles with the tLyP-1 peptide may thus enhance the tumor penetration capabilities of this nanoplatform.[40,41] By utilizing both apoA-1 and tLyP-1 surface modification strategies, we therefore hypothesize that we will be able to prepare dual-targeting rHDL NPs that can efficiently target and penetrate tumors, thereby delivering therapeutic compounds directly into transformed cells.

Herein, we prepared tLyP-1 peptide-decorated rHDL particles loaded with PTX and GANT61 in an effort to better treat metastatic TNBC. For this approach, hydrophobic GANT61 and PTX were passively encapsulated into liposomal nanoparticles (LNPs) (Scheme 1A). ApoA-1 protein self-assembly then facilitated the reconstruction of coloaded liposomes to yield rHDL NPs, with tLyP-1 peptides that were covalently bonded to cholesterol being inserted into these NPs.[25] We speculated that the intravenous delivery of these tLyP-rHDL-PTX/GANT61 NPs might enable them to preferentially accumulate within tumors owing to their superior ability to target and penetrate these malignant growths, improving the ability of drugs to diffuse into the extravascular tumor parenchyma and deep within tumors. Simultaneous GANT61 and PTX delivery have the potential to enhance anticancer therapeutic efficacy by targeting both primary tumor and metastatic processes through the stabilization of microtubules and the regulation of multiple metastasis-related targets. As such, we explored the properties, encapsulation efficiencies, and release profiles of tLyP-1-rHDL-PTX/GANT61 NPs. For these experiments, TNBC cells (MDA-MB-231, BT-549) and spheroid tumor models derived therefrom were used for *in vitro* analyses to assess the targeting and penetration efficiency of these NPs,[42,43] after which systematic *in vitro* and *in vivo* experiments were performed to evaluate their ability to suppress both primary tumor growth and metastasis. Herein, tLyP-1-rHDL NPs were therefore utilized as a promising drug-delivery system to simultaneously administer PTX and GANT61. Overall, this novel therapeutic approach has the potential to improve TNBC patient outcomes while minimizing the risk of tumor metastasis or treatment-related toxicity.

2. MATERIALS AND METHODS

2.1. Materials. Soybean phosphatidylcholine (SPC) and cholesterol were obtained from Xi'an Ruixi Biological Technology Co., Ltd. (Xi'an, China). tLyP-1 (CGNKRTR) peptide-decorated cholesterol was synthesized by Ontores technology Co., Ltd (Zhengjiang, China). Cholesterol esters, 4′,6-diamidino-2-phenylindole (DAPI), and 1,1′-dioctadecyl-3,3,3′,3′-tetramethylindotricarbocyanine iodide (DiR) were from Sigma-Aldrich (MO, USA). PTX, GANT61, and CCK-8 kits were from MedchemExpress (CA, USA). Recombinant human apolipoprotein A-1 and 1,1′-dioctadecyl-3,3,3′,3′-tetramethylindocarbocyanine perchlorate (DiI) were from Beyotime Biotechnology (Shanghai, China). Dulbecco's modified eagle's medium (DMEM), RPMI-1640, and fetal bovine serum (FBS) were from Gibco (CA, USA). Penicillin−streptomycin and phosphate-buffered saline (PBS) were from Boster Biology Technology (Wuhan, China). Human TNBC cell lines (MDA-MB-231 and BT-549) were obtained from the Cell Bank of Shanghai Institute of Biochemistry and Cell Biology, Chinese Academy of Sciences (Shanghai, China). EGF and basic fibroblast growth factor (bFGF) were from Peprotech (NJ, USA). Ethanol and trichloromethane were from Chongqing Chuandong Chemicals (Chongqing, China). Radioimmunoprecipitation assay buffer (RIPA), sodium dodecyl sulfate−polyacrylamide gel electrophoresis (SDS-PAGE), and phenylmethanesulfonyl fluoride (PMSF) were from Beyotime Biotechnology (Shanghai, China). The polyvinylidene fluoride (PVDF) membrane was from Sigma-Aldrich (MO, USA). Rabbit antibodies against Shh (ab53281), Gli1 (ab134906), CD31 (ab28364), GAPDH (ab9484), Ki67 (ab16667), SR-B1 (ab217318), and NRP-1 (ab81321) were purchased from Abcam (Cambridge, MA, USA). Rabbit antibodies against Vimentin (#5741), Snail (#3879), and E-cadherin (#3195) were obtained from Cell Signaling Technology (Danvers, MA, USA). Other reagents utilized herein were of analytical grade.

2.2. tLyP-1-rHDL-PTX/GANT61 NP Preparation. The tLyP-1-rHDL-PTX/GANT61 NPs were prepared *via* a thin-film hydration approach as detailed previously.[25,26,44] Briefly, SPC, cholesterol-tLyp, and cholesteryl ester (10:3:4 by weight) were dissolved with chloroform at an SPC concentration of 1 mg/mL and were combined with an ethanol solution containing PTX and GANT61 (SPC:PTX:GANT61 at 10:0.5:1.6 by weight) to prepare an oil phase. A thin film was then generated *via* the vacuum evaporation of the oil phase using a 37 °C water bath. PBS (pH 7.4) was then added as an aqueous phase to hydrate the film following thorough organic solvent removal. The isolated solution was then sonicated while in an ice bath and was coincubated for 24 h with apoA-1 protein at 4 °C to form tLyP-1-rHDL-PTX/GANT61 NPs. Fluorescent NPs were prepared by combining 10 μL of the DiI or DiR fluorescent dye with the lipid solution prior to film formation while protected from light.[41]

2.3. Particle Size, ζ Potential, and Morphological Analyses. The hydrodynamic diameters, polydispersity index (PDI), and ζ potential values of tLyP-1-rHDL-PTX/GANT61 NPs, tLyP-1-LNP-PTX/GANT61 NPs, rHDL-PTX/GANT61, and LNP-PTX/GANT61 NPs were established with a Zeta-Sizer Nano ZS instrument (Malvern Instruments Ltd., UK) based on dynamic light scattering, while the morphological characteristics of these particles were evaluated *via* transmission electron microscopy (TEM) (H-600, Hitachi, Japan).

2.4. Hemolysis Assay. Hemolysis studies were used to evaluate the safety of tLyP-1-rHDL-PTX/GANT61 upon intravenous injection.[45] Fresh rabbit red blood cells (RBCs) were obtained *via* centrifugation (2500 rpm, 15 min, 4 °C) and washed thrice with PBS (pH 7.4) until supernatants were clear. A 10% (v/v) RBC suspension was then prepared in PBS, with 5 mL of this 10% RBC suspension then being transferred into individual clean test tubes to which 1 mL volumes of different PTX formulations were added (final volume: 6 mL). Deionized water and PBS were also added to appropriate tubes as positive and negative controls, respectively. Tubes were incubated for 120 min at 37 °C, and then, hemoglobin absorbance in the supernatant was analyzed *via* spectrophotometric analysis at a wavelength of 540 nm. The degree of hemolysis was determined as follows: hemolysis (%)=$(A_S - A_{C+})/(A_{100\%} - A_{C-})$. A_S, A_{C+}, and A_{C-} correspond to the UV absorbance value of the experimental groups, the positive control group, and the negative control group, respectively.

2.5. Encapsulation Efficiency, Loading Efficiency, and *In Vitro* Drug Release Assays. High-performance liquid chromatography (HPLC) was used to assess PTX and GANT61 encapsulation efficiency in tLyP-1-rHDL NPs.[16,26] Briefly, samples were passed through a 0.40 μm polycarbonate membrane filter (Sigma-Aldrich, MO, USA) to remove free drug,[25] after which demulsification was conducted and PTX and GANT61 quantities in tLyP-1-rHDL-PTX/GANT61 NPs were assessed *via* HPLC (LC-10AT, Shimadzu, Japan). Encapsulation efficiency (EE %) was calculated as follows: EE % = E/$T \times 100\%$, where E and T, respectively, correspond to the amount of PTX or GANT61 in NP preparations and the total amount of these

https://doi.org/10.1021/acsami.1c02074
ACS Appl. Mater. Interfaces 2021, 13, 35248−35265

drugs. Loading efficiency (LE %) was calculated as follows: LE % = E/$W \times 100\%$, where E and W, respectively, correspond to the amount of PTX or GANT61 in NP preparations and the total weight of NPs. PTX and GANT61 release profiles from tLyP-1-rHDL-PTX/GANT61 NPs were assessed in PBS at pH values of 5.5 and 7.4. Briefly, 2 mL of tLyP-1-rHDL-PTX/GANT6 containing 0.5 mg of PTX was added to a dialysis tube (MWCO = 10 kDa, Solarbio, Beijing, China). These dialysis tubes were then added to a 100 mL volume of an appropriate release buffer and were incubated for 48 h at 37 °C with gentle agitation. At sequential time points, 0.1 mL samples of the release medium were collected and replaced with an equivalent volume of fresh medium. Isolated supernatant samples were assessed *via* HPLC to measure GANT61 and PTX levels therein.

2.6. Cell Culture. Cells were grown in DMEM and RPMI-1640 containing 10% FBS in 5% CO_2 at 37 °C incubators. Cells were regularly tested and found to be free of mycoplasma contamination. Tumorspheres were prepared by plating these cells in ultralow attachment dishes (Corning, USA) in serum-free DMEM/F12 medium (Gibco, USA) containing a hormone B27 mixture (Gibco), 20 ng/mL EGF, 10 ng/mL bFGF (Peprotech, NJ, USA), and 1 μg/mL heparin. Following a 10 day incubation under these conditions, tumorspheres were harvested.[46,47]

2.7. Assessment of Targeting and Penetration Efficiency. Cells were added to confocal dishes (NEST Biotechnology, Jiangsu. China) for 24 h, after which they were incubated with 200 μg/mL of different DiI-labeled NP preparations. In qualitative studies, cells were then washed thrice using PBS and fixed with 4% paraformaldehyde for 20 min, and nuclei were then stained using DAPI (0.5 μg/mL) for 10 min. Cells were then evaluated *via* confocal laser scanning microscopy (CLSM) (A1R-si; Nikon, Tokyo, Japan). For specific experiments, cells were added to six-well plates for 24 h, after which they were treated with DiI-labeled NPs for 1 h as mentioned above. In quantitative studies, cells were rinsed, harvested, and assessed *via* flow cytometry (NovoCyte, ACEA Biosciences, CA, USA). For the tumor spheroid penetration efficiency assessment, 3D MDA-MB-231 and BT-549 tumor spheroids were prepared as mentioned above. They were then treated with a range of DiI-labeled NP formulations (200 μg/mL) for 6 h, after which fluorescence intensity at different depths was assessed *via* CLSM.[41]

2.8. Assessment of *In Vivo* NP Distributions. The Ethics Committee of Chongqing Medical University approved all animal studies, which were consistent with the guidelines of the National Institutes of Health. Female NCG mice (6 weeks) were obtained from GemPharmatech Co. Ltd. (Nanjing, China). MDA-MB-231 cells were suspended in a 1:1 Matrigel/PBS solution (2.0×10^6 cells in 100 μL) and were injected into the mammary fat pads of mice. When tumors had grown to approximately 100 mm^3 in size, the mice were randomized into four groups (n = 5) and administered DiR-labeled LNP-PTX/GANT61, rHDL-PTX/GANT61, tLyP-1-LNP-PTX/GANT61, or tLyP-1-rHDL-PTX/GANT61 preparations *via* the tail vein. *In vivo* DiR fluorescence images were taken at 2, 6, 12, and 24 h postinjection using a small-animal *in vivo* imaging system (IVIS) (NightOWL II LB 983, Berthold, USA) to evaluate the distribution and tumor-targeting efficiency of different NPs. After 24 h, mice were sacrificed and tumors and major organs (heart, liver, spleen, lungs, and kidneys) were collected for *ex vivo* imaging.

2.9. Apoptosis and Viability Assays. Cells were added to 96-well plates and treated with free PTX and GANT61, LNP-PTX/GANT61, rHDL-PTX/GANT61, tLyP-1-LNP-PTX/GANT61, or tLyP-1-rHDL-PTX/GANT61 in a range of concentrations and at a 1:3 PTX to GANT61 ratio for 48 h. Proliferation was then assessed with a CCK-8 kit. Briefly, 100 μL of CCK-8 solution (10%) was added per well at appropriate time points. Wells were then incubated at 37 °C, after which absorbance at 450 nm was assessed *via* a plate reader. Measurements were conducted in triplicate. To assess apoptosis, cells were plated in six-well plates for 24 h, after which they were treated for 48 h with appropriate drug formulations at a PTX equivalent dose of 5 ng/mL. Cells were then harvested, and flow cytometry was used to assess cell viability (NovoCyte, ACEA Biosciences, CA, USA)

2.10. Bioinformatics Analysis. RNA-seq data and patient prognostic data were obtained from Gene Expression Omnibus data sets. The Kaplan–Meier Plotter tool[48] was used to conduct survival analyses comparing outcomes between patients with high and low levels of GLI1 expression, with median GLI1 expression levels being used to stratify patients into these two groups.

2.11. Western Blotting. RIPA containing 1% PMSF was used to extract total protein from TNBC cells, after which samples were separated *via* 10 or 15% SDS-PAGE and transferred to 0.22 μm PVDF membranes. Blots were then blocked for 2 h with a solution containing bovine serum albumin, followed by overnight incubations with primary antibodies. Blots were then probed with secondary antibodies (Cell Signaling Technology, MA, USA) for 30 min at room temperature, after which protein bands were identified through densitometric analyses (Quantity One Software; Bio-Rad, Hercules, CA).

2.12. Quantitative Polymerase Chain Reaction. Trizol (TAKARA, Shiga, Japan) was used to extract RNA from TNBC cells, after which the quantitative polymerase chain reaction (qPCR) was conducted with a CFX Connect Real-time System (Bio-Rad, CA, USA) using SYBR Green (TAKARA). Relative gene expression was assessed *via* the $2^{-\Delta\Delta CT}$ method.

2.13. *In Vitro* Cell Migration and Invasion Assay. For wound healing assays, cells were added to six-well plates and grown until confluent, at which time monolayers were wounded with sterile 200 μL pipette tips. Detached cells were removed by washing thrice with PBS, and cells were then treated with GANT61, LNP-GANT61, tLyP-1-LNP-GANT61, rHDL-GANT61, and tLyP-1-rHDL-GANT61 at a GANT61 equivalent dose of 2 μg/mL, with untreated cells serving as controls. Cells were imaged *via* an inverted microscope (BX53, Olympus, Japan) after 0 and 24 h to assess wound closure. In transwell assays, cells were added to six-well plates and grown for 1 day, after which they were treated for 48 h as mentioned above with appropriate formulations at a GANT61 equivalent dose of 2 μg/mL. Next, cells were added to the transwell insert and incubated for 24 h. Inserts were then fixed with formalin and stained with crystal violet, and migration was assessed *via* microscopy. In invasion experiments, experimental methods were the same except that cells were added to Matrigel (BD Bioscience, NY, USA)-coated inserts.

2.14. Tube Formation Assay. MDA-MB-231 and BT-549 cells were plated in six-well plates and grown to 90% confluence, at which time they were treated for 48 h with appropriate formulations (GANT61 equivalent dose of 2 μg/mL). Cells were then washed with PBS and grown in serum-free media for 24 h. Supernatants were then isolated from these cells and used as conditioned media to culture human umbilical vein endothelial cells (HUVECs) in 48-well plates (2×10^4 cells/well) that had been coated with 100 μL of Matrigel (BD Biosciences, MA, USA). Cells were regularly imaged with an inverted microscope (Olympus, Shinjuku, Tokyo, Japan) during treatment and were imaged at a 4 h time point.

2.15. Tumor Spheroid Formation Assay. MDA-MB-231 and BT-549 cells were cultured for 48 h with different groups of formulations (at a GANT61 equivalent dose of 2 μg/mL). Next, cells (1×10^4 cells/mL) were added to ultralow attachment six-well-plates in serum-free DMEM/F12 medium containing hormone mixture B27, 20 ng/mL EGF, 10 ng/mL bFGF, and 1 μg/mL heparin in a 5% CO_2 incubator at 37 °C for 10 days. Tumorspheres >75 μm in size were then counted *via* microscopy.[46,47]

2.16. *In Vivo* Antitumor Efficacy and Toxicity Analyses. The Ethics Committee of Chongqing Medical University approved all animal studies, which were consistent with the guidelines of the National Institutes of Health. A spontaneous breast cancer metastasis model was established as previously described.[49] MDA-MB-231 cells expressing luciferase were suspended in a 1:1 Matrigel/PBS solution (2.0×10^6 cells in 100 μL) and were injected into the mammary fat pads of NCG mice. Tumors were allowed to grow until approximately 100 mm^3 in size, at which time mice were randomized into eight treatment groups (n = 5/group) and intravenously administered saline, PTX, GANT61, PTX + GANT61, LNP-PTX/GANT61, rHDL-PTX/GANT61, tLyP-1-LNP-PTX/GANT61, or tLyP-1-

https://doi.org/10.1021/acsami.1c02074
ACS Appl. Mater. Interfaces 2021, 13, 35248−35265

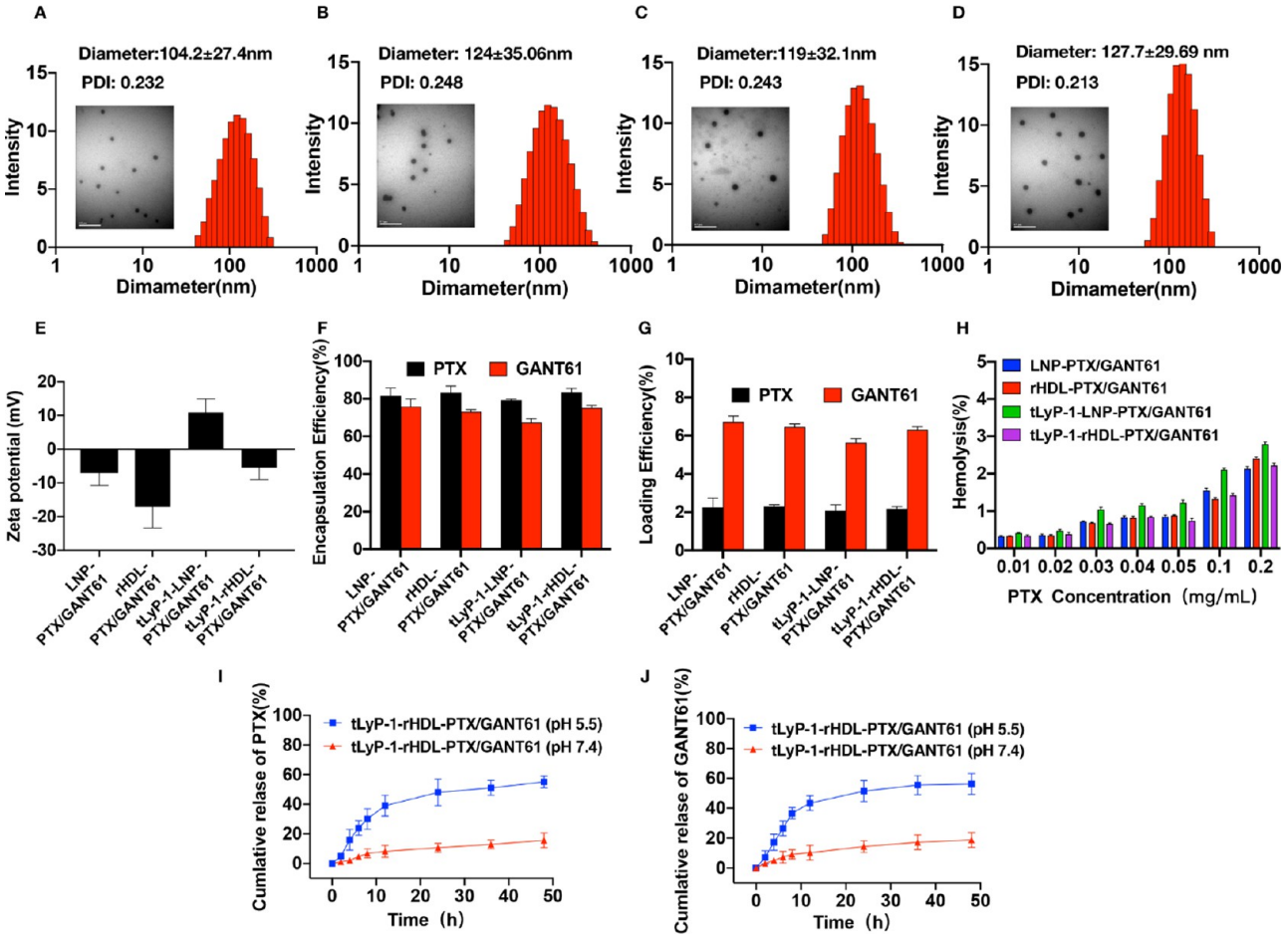

Figure 1. LNP-PTX/GANT61, rHDL-PTX/GANT61, tLyP-1-LNP-PTX/GANT61, and tLyP-1-rHDL-PTX/GANT61 NP characterization. Size distributions and TEM images of (A) LNP-PTX/GANT61, (B) rHDL-PTX/GANT61, (C) tLyP-1-LNP-PTX/GANT61, and (D) tLyP-1-rHDL-PTX/GANT6 NPs. Scale bar: 500 nm. (E) ζ potential values of different groups of NPs were measured *via* DLS. PTX and GANT61 (F) encapsulation efficiencies and (G) loading efficiencies for different groups of NPs. (H) Hemolysis of tested formulations at various concentrations. (I) Cumulative PTX and (J) GANT61 release curves for tLyP-1-rHDL-PTX/GANT61 in solutions of PBS under different pH (7.4 and 5.5), respectively (data are means ± S.D., $n = 3$).

rHDL-PTX/GANT61 (7 mg/kg PTX and 21 mg/kg GANT61) preparations on days 14, 17, 20, 23, 26, and 29 postimplantation. Tumor sizes and body weight values were monitored immediately prior to dosing, with tumor volume being determined as follows: volume (mm^3) = length × $width^2/2$. On days 1, 30, and 40 postimplantation, bioluminescent images were captured. Briefly, mice were anesthetized and intraperitoneally injected with D-luciferin (15 mg/mL in 200 μL). Following a 15 min incubation, the IVIS system was then used to image these individual animals. A bioluminescent signal was defined based on relative optical intensity, and data were reported in terms of radiance. On day 41 postimplantation, each group of mice was euthanized, and blood samples were collected for hematological and biochemical analyses, while tumors were collected for imaging. Samples were subjected to hematoxylin and eosin (H&E) staining, Ki67 and CD31 immunohistochemical staining, and terminal deoxynucleotidyl transferase dUTP nick end labeling (TUNEL) staining. Lungs from these mice were incubated for 24 h in Bouin's solution, after which numbers of surface nodules were determined. H&E staining of major organs (lungs, kidneys, liver, spleen, and heart) was additionally conducted to assess tissue histopathology.

2.17. Statistical Analysis. Data are given as means ± standard deviation (S.D.) from three or more replicate experiments and were compared using Student's t-tests or one-way analyses of variance. Differences were considered statistically significant at $*p < 0.05$, $**p < 0.01$, and $***p < 0.001$.

3. RESULTS AND DISCUSSION

3.1. Characterization of NPs. We began by preparing tLyP-1-rHDL-PTX/GANT61 NPs *via* a thin-film hydration approach, encapsulating PTX and GANT61 into the hydrophobic core of these particles, which were subjected to surface modification with the tLyP-1 peptide and apoA-1 to facilitate dual-targeting. Subsequent TEM imaging revealed spherical NPs of uniform size, consistent with the results of Malvern ZetaSizer imaging (Figure 1A–D). Prepared tLyP-1-rHDL-PTX/GANT61, tLyP-1-LNP-PTX/GANT61, and rHDL-PTX/GANT61 NPs had slightly larger diameters than those of LNPs, likely owing to the surface apoA-1 and tLyP-1 peptide modifications. The tLyP-1-rHDL-PTX/GANT61 NPs had an average diameter of 127.7 ± 29.69 nm with a desirable PDI of 0.213, enabling them to readily pass through the tumor vascular endothelial gap (380–780 nm) into extravascular tumor tissues, thus improving drug-delivery efficiency. Relative to tLyP-1-LNP-PTX/GANT61 NPs, these tLyP-1-rHDL-PTX/GANT61 NPs also had a negative ζ potential attributable to the negative charge of apoA-1 (Figure 1E), thus rendering these particles more stable in plasma as they will be less likely to interact with plasma proteins that are negatively charged.[50,51] To assess the safety of intravenously

https://doi.org/10.1021/acsami.1c02074
ACS Appl. Mater. Interfaces 2021, 13, 35248–35265

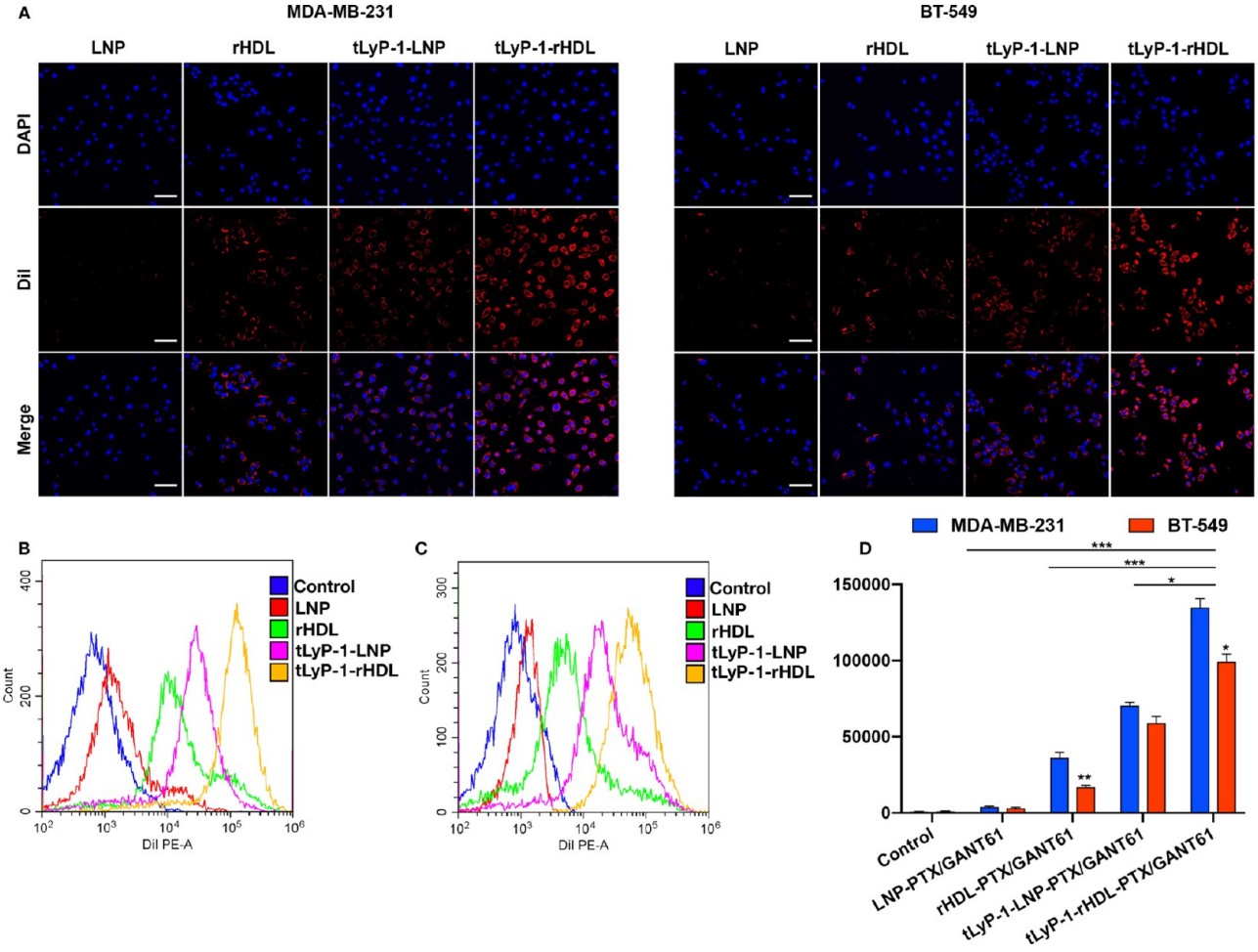

Figure 2. Analysis of DiI-labeled LNP-PTX/GANT61, rHDL-PTX/GANT61, tLyP-1-LNP-PTX/GANT61, and tLyP-1-rHDL-PTX/GANT61 NPs *in vitro* tumor-targeting efficiency. (A) DiI-labeled LNP-PTX/GANT61, rHDL-PTX/GANT61, tLyP-1-LNP-PTX/GANT61, or tLyP-1-rHDL-PTX/GANT61 NP *in vitro* tumor-targeting efficiency following a 1 h incubation with MDA-MB-231 and BT-549 cells was assessed *via* CLSM. Red and blue fluorescence corresponds to DiI and DAPI, respectively. Scale bars: 100 μm. (B) MDA-MB-231 fluorescence intensity following incubation with DiI-labeled LNP-PTX/GANT61, rHDL-PTX/GANT61, tLyP-1-LNP-PTX/GANT61, or tLyP-1-rHDL-PTX/GANT61 NPs. (C) BT-549 fluorescence intensity following incubation with DiI-labeled different groups of NPs. (D) Quantitative fluorescence intensity of DiI-labeled LNP-PTX/GANT61, rHDL-PTX/GANT61, tLyP-1-LNP-PTX/GANT61, and tLyP-1-rHDL-PTX/GANT61 NPs in MDA-MB-231 and BT-549 cells (Bar graphs with error bars indicated means ± S.D., $n = 3$, *$p < 0.05$, **$p < 0.01$, and ***$p < 0.001$).

injecting these particles, an NP hemolysis assay was performed to assess their hemocompatibility. As shown in Figure 2H, the hemolysis rate associated with PTX/GANT61-loaded formulations was less than 5%, suggesting that these tLyP-1-rHDL-PTX/GANT61 NPs exhibit satisfactory biocompatibility and can be used for intravenous injection.

Efficient drug-delivery systems must exhibit a high drug-loading efficiency and be able to release their cargos directly within target sites. We therefore next evaluated the EE % and LE % of our prepared NPs for PTX and GANT61. All tested NPs were able to effectively encapsulate both of these drugs without significant changes in EE % or LE % as a function of NP surface modifications (Figure 1F,G). The PTX and GANT61 EE % values in tLyP-1-rHDL-PTX/GANT61 NPs were 83.4 ± 2.1% and 75.2 ± 1.3%, respectively, while the LE % values of PTX and GANT61 in tLyP-1-rHDL-PTX/GANT61 NPs were 2.1 ± 0.11% and 6.3 ± 0.17%, respectively. When we assessed the release profiles for these two drugs from our tLyP-1-rHDL-PTX/GANT61 NPs, we found that in neutral (pH 7.4) PBS, just 15.6 ± 4.4 and 18.3 ± 5.1% of encapsulated PTX and GANT61, respectively, was released, whereas in acidic (pH 5.5) PBS, these NPs released 54.7 ± 3.9 and 56.2 ± 7.2% of these respective drugs (Figure 1I,J). These findings indicated that tLyp-1-rHDL-PTX/GANT61 NPs remained stable under normal physiological conditions and could release their cargo drugs within acidic conditions, in line with prior findings.[25] The apolipoprotein A-1 was the main component to stabilize the structure of rHDL NPs, which result in the excellent stability of rHDL NPs under neutral conditions.[28,52] However, the acidic environment could change the structure and function of apolipoprotein A-1, leading to loss of operation of the apolipoprotein A-1-stabilized rHDL NP.[53−55] This in terms results in a greater drug release under acidic conditions. Given that an acidic microenvironment is a common feature of many tumors owing to intratumoral anaerobic glycolysis,[56,57] such pH-responsive drug-release behavior may enhance intratumoral drug release. Owing to these abovementioned promising characteristics, our tLyP-1-rHDL-PTX/GANT61 NPs were considered to be feasible drug-delivery tools worthy of further experimental evaluation.

3.2. Targeting and Penetrating Efficiency of NPs *In Vitro*. A successful drug-delivery system must be able to

https://doi.org/10.1021/acsami.1c02074
ACS Appl. Mater. Interfaces 2021, 13, 35248−35265

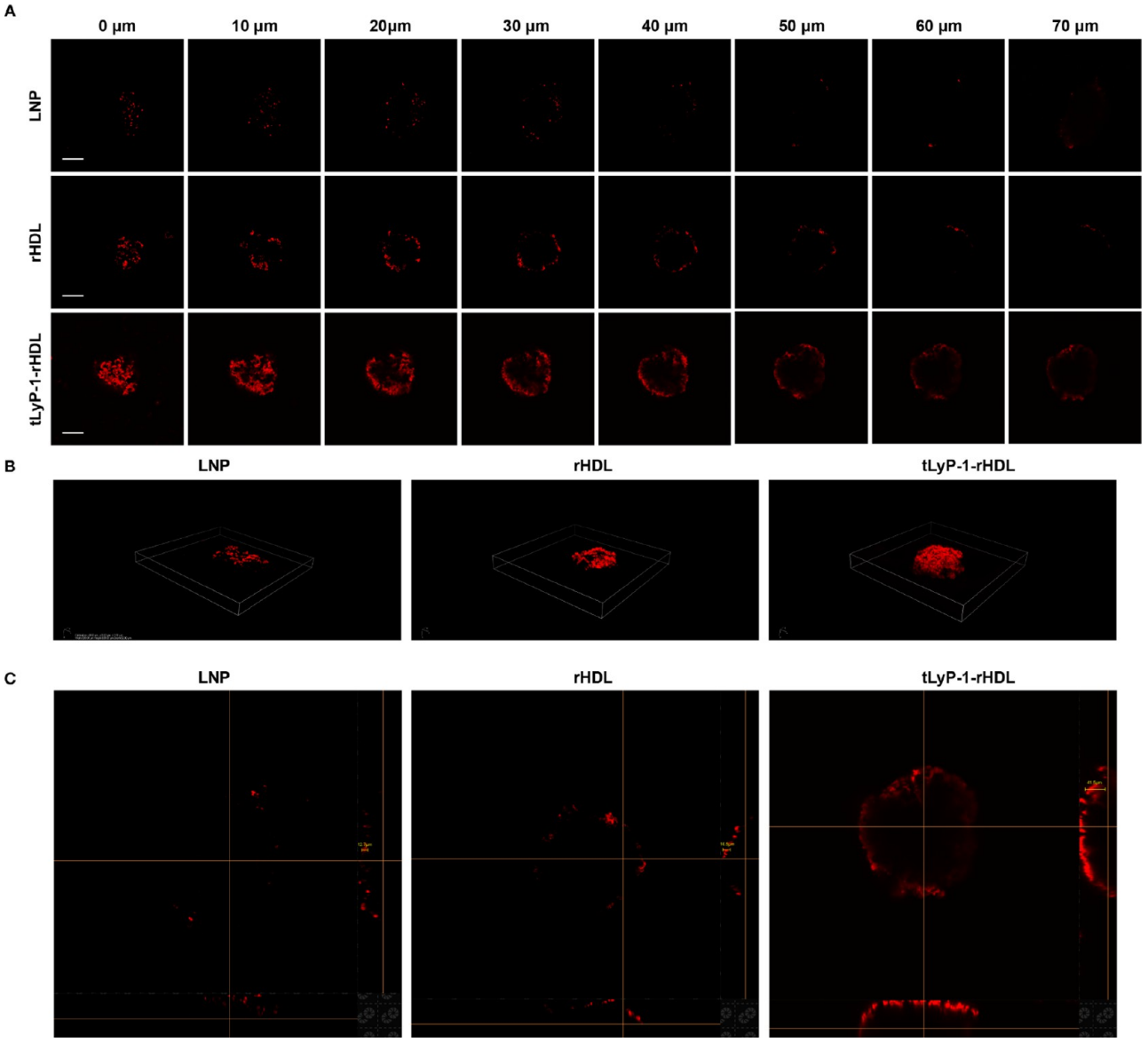

Figure 3. DiI-labeled LNP-PTX/GANT61, rHDL-PTX/GANT61, and tLyP-1-rHDL-PTX/GANT61 NP tumor penetration efficiency in MDA-MB-231 spheroids. (A) Multilevel scans were initiated at the bottom of spheroids and were conducted in 10 μm intervals to assess the penetration of DiI-labeled LNP-PTX/GANT61, rHDL-PTX/GANT61, or tLyP-1-rHDL-PTX/GANT61 NPs following a 6 h incubation. Scale bar: 100 μm. (B) Three-dimensional reconstructions of MDA-MB-231 spheroids incubated with DiI-labeled LNP-PTX/GANT61, rHDL-PTX/GANT61, or tLyP-1-rHDL-PTX/GANT61 NPs. (C) DiI-labeled LNP-PTX/GANT61, rHDL-PTX/GANT61, or tLyP-1-rHDL-PTX/GANT61 NP penetration values were quantified. Red fluorescence corresponds to Dil.

deliver therapeutic compounds directly to cells of interest through specific interactions with target cells and subsequent intracellular cargo release. Ligand-mediated targeting represents a viable approach to actively enhance drug delivery to cell types of interest, and the tLyP-1 peptide and apoA-1 modifications employed in the present study may therefore be able to enhance NP delivery to tumor cells. To explore the targeting properties of our NP preparations, we utilized MDA-MB-231 and BT-549 TNBC cells as experimental models for *in vitro* analyses. CLSM imaging revealed that DiI-labeled tLyP-1-rHDL-PTX/GANT61 NPs were able to accumulate in association with the cell membrane and cytoplasm of both of these cell lines (Figure 2A). Relative to nonmodified NPs, those with surface tLyP-1 modifications better accumulated within the cytoplasm, likely owing to the NRP-1 receptor-mediated internalization. Indeed, significantly higher levels of tLyP-1-rHDL-PTX/GANT61 NPs were associated with the cell membrane and cytoplasm of target cells relative to tLyP-1-LNP NPs, rHDL NPs, and unmodified NPs without targeting ligands. Quantitative analyses conducted *via* flow cytometry confirmed these results (Figure 2B–D). Moreover, quantitation of fluorescence by flow cytometry indicated that the targeting efficiency of rHDL-PTX/GANT61 and tLyP-1-rHDL-PTX/GANT61 NPs for MDA-MB-231 cells was significantly stronger than that for BT-549 cells. This may be attributable to differences in receptor protein expression between these two cell lines. Western blotting indicated that while NRP-1 receptor expression levels did not differ between MDA-MB-231 and BT-549 cells, the level of SR-B1 expression was higher in MDA-MB-231 cells than in BT-549 cells (Figure S1). MDA-MB-231 cells were thus more likely to bind to rHDL-PTX/GANT61 and tLyP-1-rHDL-PTX/GANT61 NPs

https://doi.org/10.1021/acsami.1c02074
ACS Appl. Mater. Interfaces 2021, 13, 35248−35265

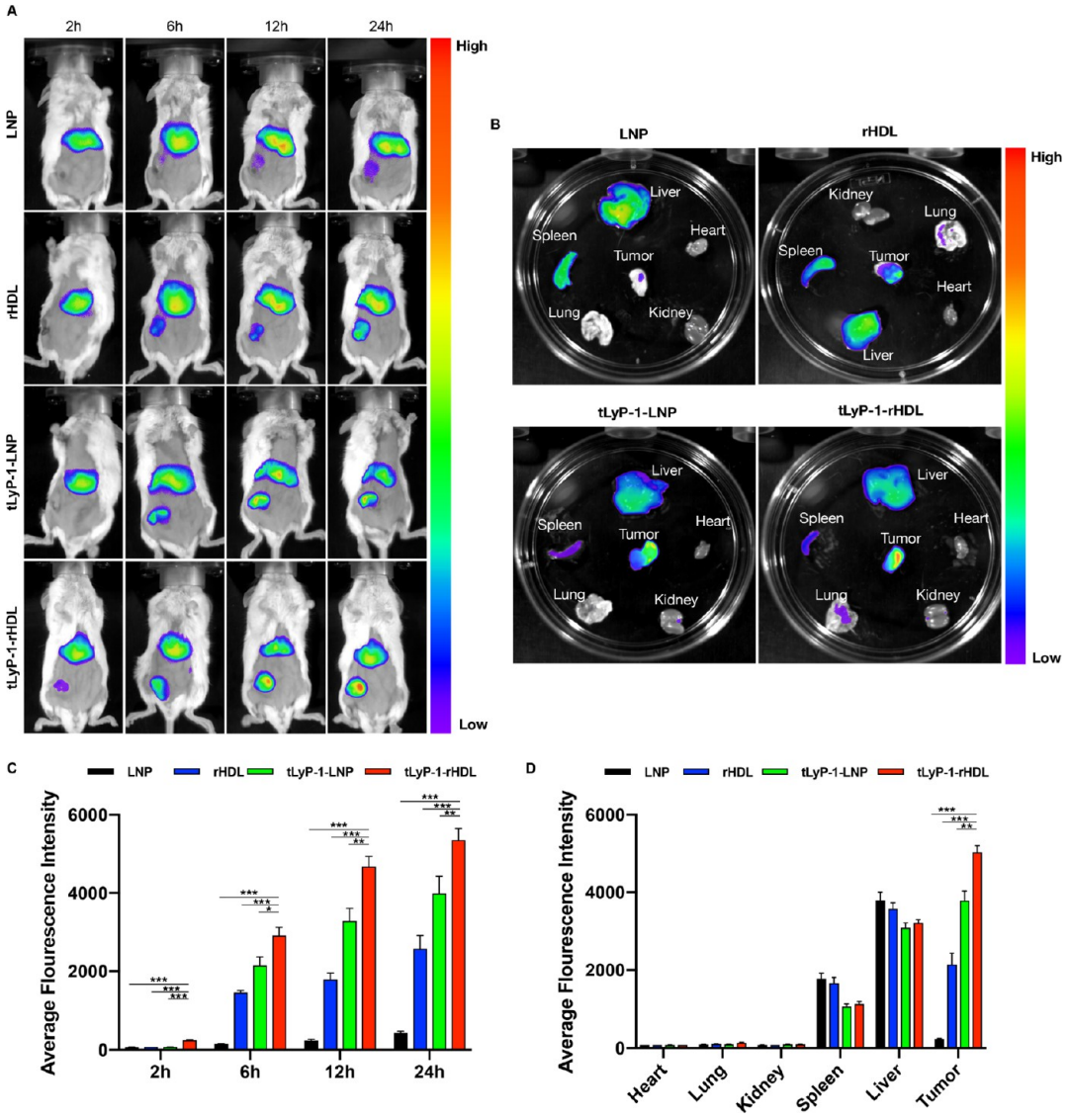

Figure 4. Assessment of the ability of DiR-labeled LNP-PTX/GANT61, rHDL-PTX/GANT61, tLyP-1-LNP-PTX/GANT61, and tLyP-1-rHDL-PTX/GANT61 to target MDA-MB-231 tumors in NCG mice. (A) Representative fluorescent time-lapse images and (C) quantified fluorescent data in MDA-MB-231 tumor-bearing NCG mice that were intravenously administered DiR-labeled NPs. (B) Representative ex vivo fluorescence images and (D) quantified fluorescent data for tumors and tissues isolated from tumor-bearing mice at 24 h post-treatment (data are means ± S.D., $n = 5$, $p < 0.05$, $^{**}p < 0.01$, and $^{***}p < 0.001$).

which were decorated with apoA-1 and were able to recognize the SR-B1 receptor.

Penetrating physiological barriers is also a reliable approach to enhance drug delivery. To explore the penetration efficiency of our tLyP-1-rHDL-PTX/GANT61 NPs, we established 3D MDA-MB-231 and BT-549 tumor spheroids to better mimic the tumor microenvironment.[47] Such spheroids have been shown to bear many similarities to the microenvironmental characteristics of solid tumors, including heterogeneous tumor perfusion, high cell density, an acidic pH, and elevated interstitial pressure.[42,43] Following a 6 h incubation of MDA-MB-231 spheroids with different DiI-labeled NPs, tLyP-1-rHDL-PTX/GANT61 NPs exhibited increased distribution levels within spheroids relative to LNP-PTX/GANT61 and rHDL-PTX/GANT61 NPs (Figure 3A). The tLyP-1-rHDL-PTX/GANT61 NPs were able to penetrate to over 41.5 μm from the bottom of the tumor spheroids, while LNP-PTX/GANT61 and rHDL-PTX/GANT61 NPs penetrated to the respective depths of just 16.5 and 12.7 μm (Figure 3B,C). In line with these results, tLyP-1-rHDL-PTX/GANT61 NPs were also better able to penetrate BT-549 spheroids than were LNP-PTX/GANT61 or rHDL-PTX/GANT61 NPs (Figure S2). These data suggest that dual-targeting tLyP-1-rHDL NPs were able to target the SR-B1 or NRP-1 receptors on TNBC cells with high efficiency, thereby improving tumor cell recognition and intracellular drug release, which is essential to facilitate tumor-specific NP delivery *in vivo*. The tLyP-1 peptide was thus able to improve NP penetration deep within tumor-spheres, increasing the number of tumor cells likely to be encountered by these NPs and thereby enhancing cargo delivery efficiency.

3.3. *In Vivo* Biodistribution. Tumor-specific drug accumulation represents the most efficient means of killing tumor cells while reducing systemic toxicity. We therefore tested the ability of our different NP formulations to facilitate intratumoral drug accumulation in MDA-MB-231 tumor-

https://doi.org/10.1021/acsami.1c02074
ACS Appl. Mater. Interfaces 2021, 13, 35248−35265

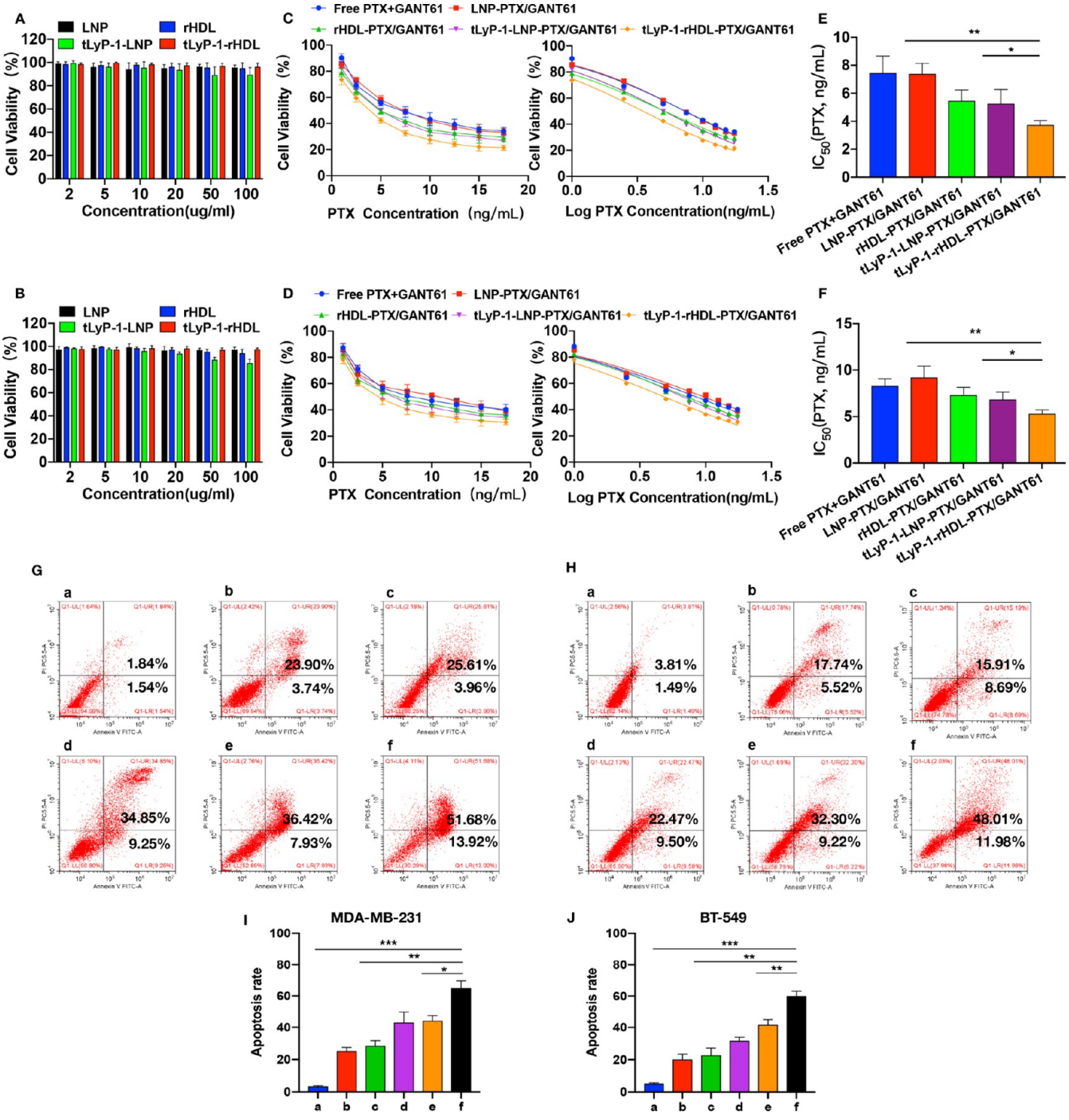

Figure 5. Evaluation of *in vitro* antitumor efficacy. The viability of (A) MDA-MB-231 cells and (B) BT-549 cells exposed to different concentrations of LNP, rHDL, tLyP-1-LNP, or tLyP-1-rHDL NPs for 48 h. The viability of (C) MDA-MB-231 and (D) BT-549 breast cancer cells following treatment with NPs or free drug solutions at PTX-to-GANT61 mass ratios of 1:3 was assessed *via* CCK-8 assay and the IC50 fitting curve. IC50 of free PTX + GANT61 and different formations in (E) MDA-MB-231 and (F) BT-549 cells. MDA-MB-231 (G) and BT-549 (H) cell apoptosis at 48 h following treatment with the indicated formulations was assessed *via* flow cytometry. (a) Control, (b) free PTX + GANT61, (c) LNP-PTX/GANT61, (d) rHDL-PTX/GANT61, (e) tLyP-1-LNP-PTX/GANT61, and (f) tLyP-1-rHDL-PTX/GANT61, upper left quadrant, necrotic cells; lower left quadrant, live cells; upper right quadrant, late apoptotic cells; and lower right quadrant, early apoptotic cells. (I,J) Quantitative analysis of apoptotic cells (data are means ± S.D., $n = 3$, $^{*}p < 0.05$, $^{**}p < 0.01$, and $^{***}p < 0.001$).

bearing NCG mice. All of our NPs mediated intratumoral drug accumulation in a time-dependent manner (Figure 4A,C). Interestingly, even without targeting ligands, a small amount of LNP-PTX/GANT61 NPs was detectable within the tumor site. This is likely attributable to the enhanced permeability and retention (EPR) effect. However, consistent with previous studies, the EPR-mediated aggregation of NPs in tumor tissues was minimal.[58] Compared with LNP NPs, the rHDL-PTX/GANT61 and tLyP-1-LNP-PTX/GANT61 NPs bearing targeting ligands exhibited significantly increased accumulation in the tumor site. This suggested that these targeting ligands were able to enhance active targeting efficiently to ensure

https://doi.org/10.1021/acsami.1c02074
ACS Appl. Mater. Interfaces 2021, 13, 35248−35265

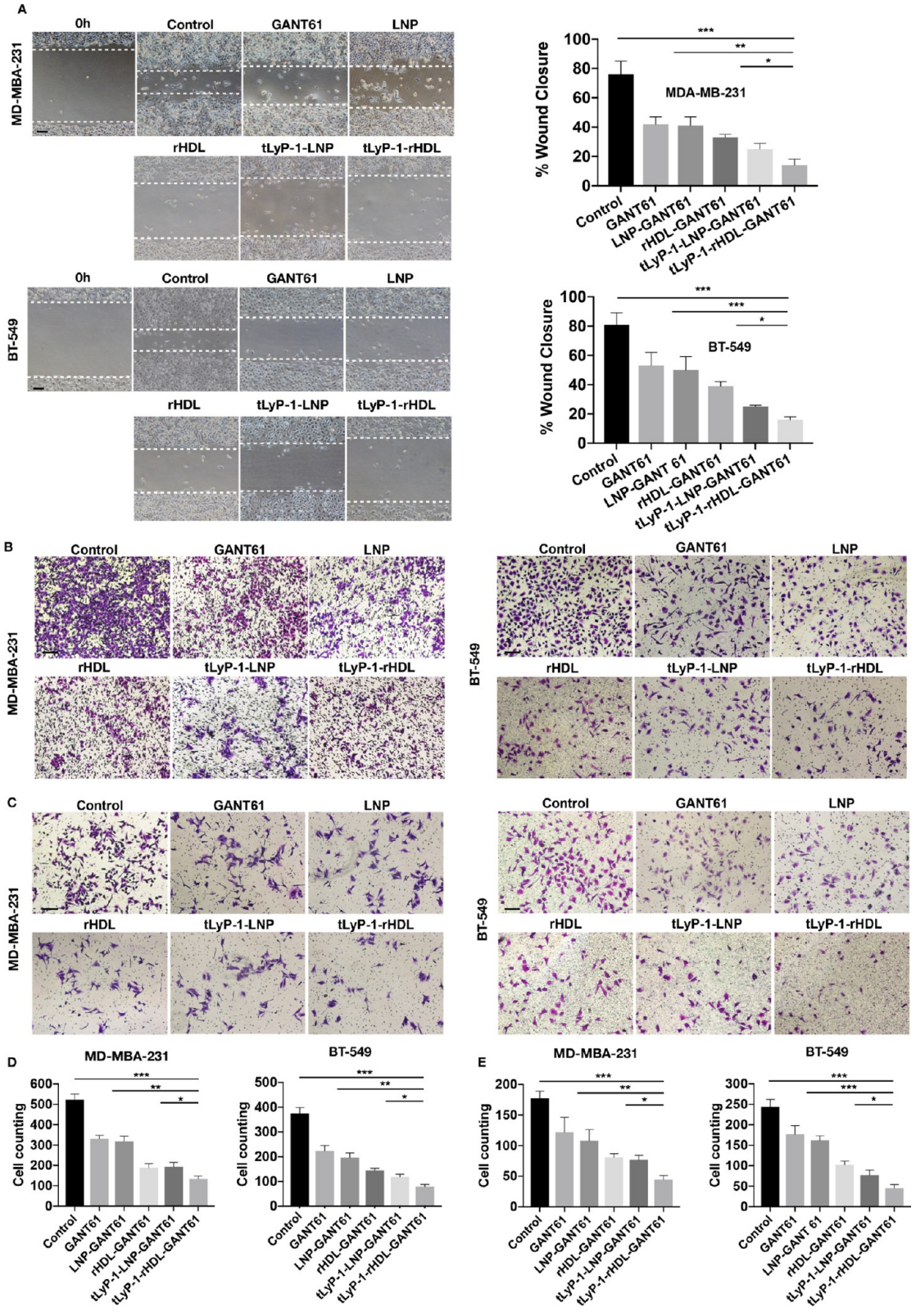

Figure 6. Assessment of the ability of different formulations to inhibit MDA-MB-231 and BT-549 cell migration and invasion. Representative images of (A) wound healing, (B) migration, and (C) invasion analyses for cells treated by GANT61(5 μg/mL), LNP-GANT61, rHDL-GANT61, tLyP-1-LNP-GANT61, and tLyP-1-rHDL-GANT61. (D,E) Migratory and invasive activity of MDA-MB-231 and BT-549 cells in the lower chamber was quantified (scale bars:100 μm, bar graphs with error bars indicated means ± S.D., n = 3, *p < 0.05, **p < 0.01, and ***p < 0.001).

tumor-specific drug delivery. Moreover, the tLyP-1-rHDL-PTX/GANT61 NPs with dual-targeting properties exhibited significantly improved accumulation within tumors relative to rHDL-PTX/GANT61, tLyP-LNP-PTX/GANT61 NPs, and NPs lacking any targeting ligands, as determined based on analyses of intratumoral fluorescence. This is likely a

https://doi.org/10.1021/acsami.1c02074
ACS Appl. Mater. Interfaces 2021, 13, 35248−35265

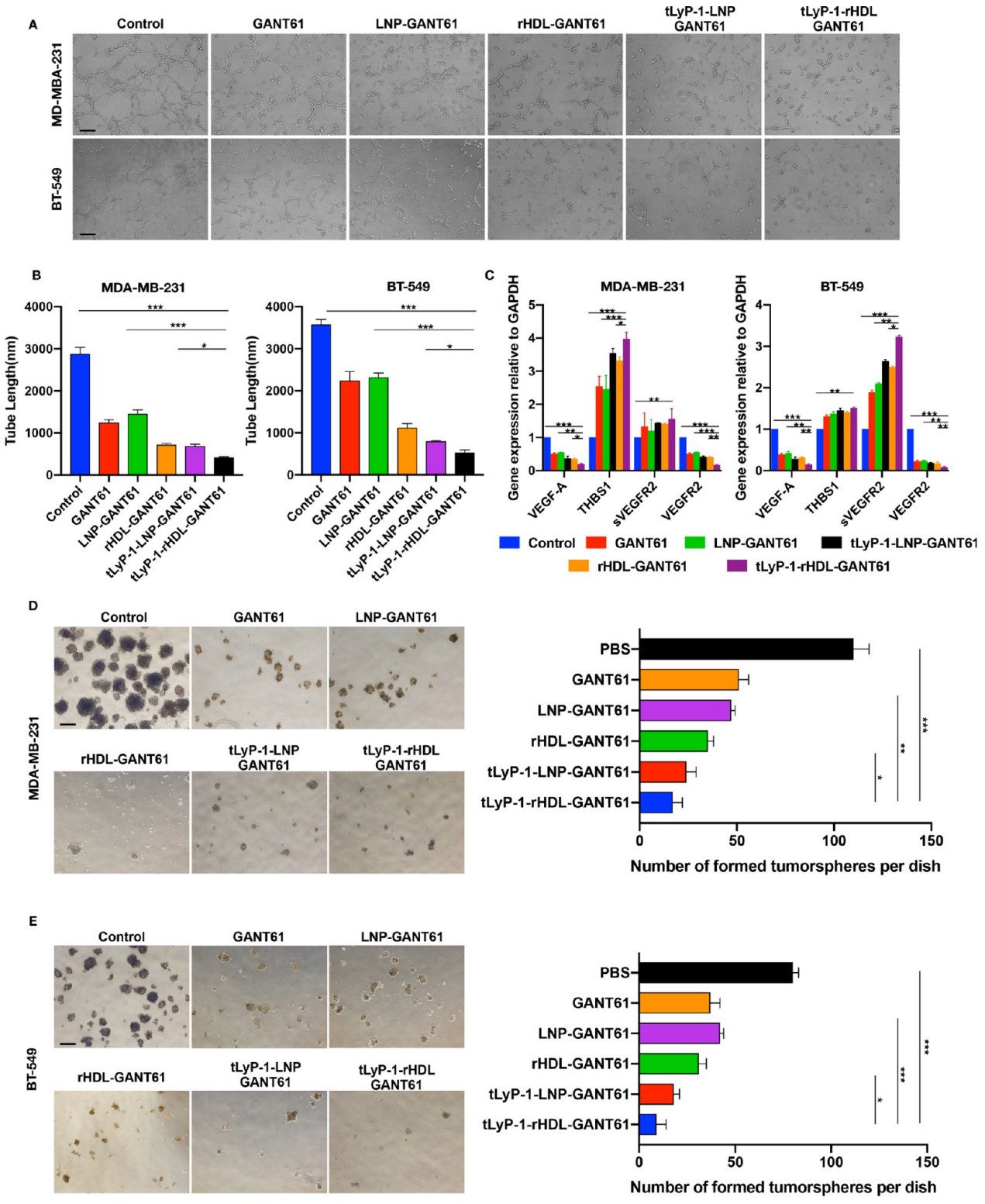

Figure 7. Assessment of the ability of various formulations to suppress MDA-MB-231 and BT-549 angiogenic activity and stemness. (A,B) Representative images and quantitative analyses of HUVEC tube formation following growth in medium isolated from MDA-MB-231 and BT-549 cells treated with GANT61 (5 μg/mL), LNP/GANT61, rHDL/GANT61, tLyP-1-LNP/GANT61, or tLyP-1-rHDL/GANT61 for 48 h. (C) Relative VEGF-A, THBS1, sVEGFR2, and VEGFR2 mRNA levels of MDA-MB-231 and BT-549 cells subjected to the indicated treatments were assessed *via* qPCR. (D,E) Representative images and quantitative analyses of MDA-MB-231 and BT-549 tumorsphere formation after treatment with different formations (scale bars:100 μm, bar graphs with error bars indicated means ± S.D., $n = 3$, $^{*}p < 0.05$, $^{**}p < 0.01$, and $^{***}p < 0.001$).

consequence of combining the active targeting activities of the tLyP-1 peptide and apoA-1. This result was further confirmed *via ex vivo* imaging (Figure 4B,D), suggesting that the ability of LyP-1-rHDL NPs to penetrate and bind the tumor parenchyma results in more efficient intratumoral accumulation. These dual-targeting tumor-penetrating tLyP-1-rHDL

https://doi.org/10.1021/acsami.1c02074
ACS Appl. Mater. Interfaces 2021, 13, 35248−35265

NPs may thus be developed as a viable drug-delivery platform for the targeted treatment of TNBC or other tumors.

3.4. Cytotoxicity Assay *In Vitro*. Clinically useful drug-delivery systems must be able to simultaneously enhance drug efficacy while maintaining biocompatibility. To this end, we employed a CCK-8 assay approach to assess the cytotoxic effects of blank and drug-loaded NPs. Consistent with prior reports, blank NPs failed to induce substantial toxicity (Figure 5A,B). At high NP doses (100 μg/mL), tLyP-1-rHDL treatment was associated with >90% viability for both cell lines, suggesting that these modified NPs represent a safe drug-delivery platform. Importantly, all free drug solutions and drug-loaded NPs exhibited dose-dependent suppressive effects on tumor cell proliferation (Figure 5C,D). Relative to free PTX and GANT61 cocktails, tLyP-1-rHDL-PTX/GANT61 NPs were better able to suppress the proliferation of both tested TNBC cell lines, with significantly lower IC_{50} values than those for free drug solutions, tLyP-1-LNP NPs, or rHDL NPs (Figure 5E,F). Flow cytometry analyses were then conducted to further evaluate the cytotoxic effects of tLyP-1-rHDL-PTX/GANT61 NP treatment, similarly revealing these drug-loaded NPs to induce apoptosis more efficiently than other tested treatments (Figure 5G–J). This suggested that tLyP-1-rHDL-PTX/GANT61 NPs can readily induce the cytotoxic death of TNBC cells more effectively than free PTX and GANT61 solutions, likely owing to the functionalization of these NPs with our dual-targeting ligands and the resultant enhancement of PTX and GANT61 accumulation within tumor cells.[59,60]

3.5. Bioinformatics Mining and GLi1 Suppression Efficiency of NPs. Prior work has shown that the SHH signaling pathway is excessively activated in TNBC tumors. The GLI1 transcription factor is an SHH pathway effector that controls key downstream genes associated with angiogenesis and the epithelial–mesenchymal transition (EMT), thereby regulating tumor metastasis and patient prognosis.[9−13] Bioinformatics analyses revealed that elevated GLI1 expression was associated with poorer OS, disease-free survival (DFS), and recurrence-free survival (RFS) in the GSE16446 and GSE7390 data sets as compared to low GLI1 expression (Figure S3A). The Kaplan–Meier plotter database was additionally used to analyze multiple TNBC patient data sets, confirming high GLI1 expression to be associated with poorer DFS and RFS (Figure S3B). This suggests that GLI1 may be a viable therapeutic target in TNBC patients. We therefore assessed the inhibitory impact of our NPs on GLI1 expression *via* Western blotting (Figure S3C), revealing that GANT61 treatment suppressed the expression of this protein in both TNBC cell types, and NP targeting enhanced this inhibitory activity, with the tLyP-1-rHDL-GANT61 NPs exhibiting the most significant inhibitory effect of these different formulations.

3.6. Antimigration and Invasion Efficiency of NPs *In Vitro*. Given that we found that our different NP formulations were able to suppress GLI1 in TNBC cells, we next assessed the impact of these treatments on activities regulated by this transcription factor including cell migration and invasion *via* wound healing and transwell assays. In a wound healing assay, both tested TNBC cell types exhibited substantial metastatic activity. Relative to cells treated with GANT61, those treated with different NPs exhibited more potent suppression of tumor cell migration, with tLyP-1-rHDL NPs exhibiting the most significant inhibition of wound closure (Figure 6A), which was reduced to just 14 and 17% of that in control groups for MDA-MB-231 and BT-549 cells, respectively. Consistent with these findings, tLyP-1-rHDL-GANT61 NPs exhibited significantly better antimigratory (Figure 6B,D) and anti-invasive (Figure 6C,E) activity in transwell assays relative to free GANT61, nontargeting NPs, rHDL-GANT61, and tLyP-1-LNP-GANT61. To further explore the mechanisms governing the suppression of tumor cell invasion and metastasis in these different treatment groups, we assessed the levels of EMT-related proteins including E-cadherin, Vimentin, and Snail *via* Western blotting. Following GANT61 treatment, E-cadherin was elevated while the levels of these other two proteins were reduced (Figure S4). Consistent with the abovementioned data, the tLyP-1-rHDL-GANT61 NPs exhibited to most robust ability to alter EMT-related protein expression in these different treatment groups, suggesting that these dual-targeting NPs can effectively modulate EMT-related protein expression by suppressing GLI1, thereby inhibiting TNBC cell migration and invasion.

3.7. *In Vitro* Tube Formation and Tumorsphere Formation Assay. The GLI1 transcription factor targets a number of different genes associated with tumor metastasis and phenotypic traits.[13,61] GANT61 can not only inhibit tumor cell invasion and migration but also interfere with TNBC cell stemness and angiogenesis.[13] As such, we next evaluated the effects of our various NP formulations on tube formation and tumorsphere development *in vitro*. For tube formation assays, we utilized HUVECs grown in conditioned medium isolated from MDA-MB-231 and BT-549 cells following treatment with free GANT61 or different NP formulations. As predicted, dual-targeting tLyP-1-rHDL-GANT61 treatment was sufficient to disrupt HUVEC tube formation more readily than other treatments (Figure 7A,B). Consistent with this, when we assessed the mRNA levels of angiogenesis-related factors including VEGFR2, THBS1, sVEGFR2, and VEGF-A *via* qPCR, we found that the levels of the endogenous angiogenesis inhibitors sVEGFR2 and THBS1 were significantly increased,[13] while the levels of proangiogenic VEGF-A and VEGFR2 were reduced (Figure 7C). Importantly, tLyP-1-rHDL-GANT61 NPs exhibited more potent effects relative to GANT61, rHDL-GANT61, or tLyP-LNP-GANT61 treatment.

Tumorsphere formation assays were additionally employed to assess how GANT61-loaded NPs were able to influence cancer stemness. GANT61 suppressed the formation of these spheroids for both tested cell lines, underscoring the therapeutic value of GLI1 suppression as a means of inhibiting tumor stem cell growth.[46,61] Our targeted NPs loaded with GANT61 were even more effective inhibitors of tumorsphere formation relative to free GANT61, with few such spheres being detectable following rHDL-GANT61 and tLyP-1-LNP-GANT61 treatment and with even fewer being present following tLyP-1-rHDL-GANT61 NP treatment (Figure 7D,E). These data suggested that GANT61 can regulate a number of target genes associated with angiogenesis, suppressing such an activity. The dual-targeting tLyP-1-rHDL NP delivery system further enhanced GANT61 accumulation within tumor cells, thereby more effectively inhibiting TNBC cell malignancy, highlighting this as a promising approach to inhibit cancer metastasis *in vivo*.

3.8. *In Vivo* Therapeutic Efficacy. To additionally confirm the functionality and synergistic activity of tLyP-1-rHDL-PTX/GANT61-based TNBC treatment, we evaluated the ability of these NPs to treat both primary tumors and metastases using the highly metastatic orthotopic MDA-MB-

https://doi.org/10.1021/acsami.1c02074
ACS Appl. Mater. Interfaces 2021, 13, 35248−35265

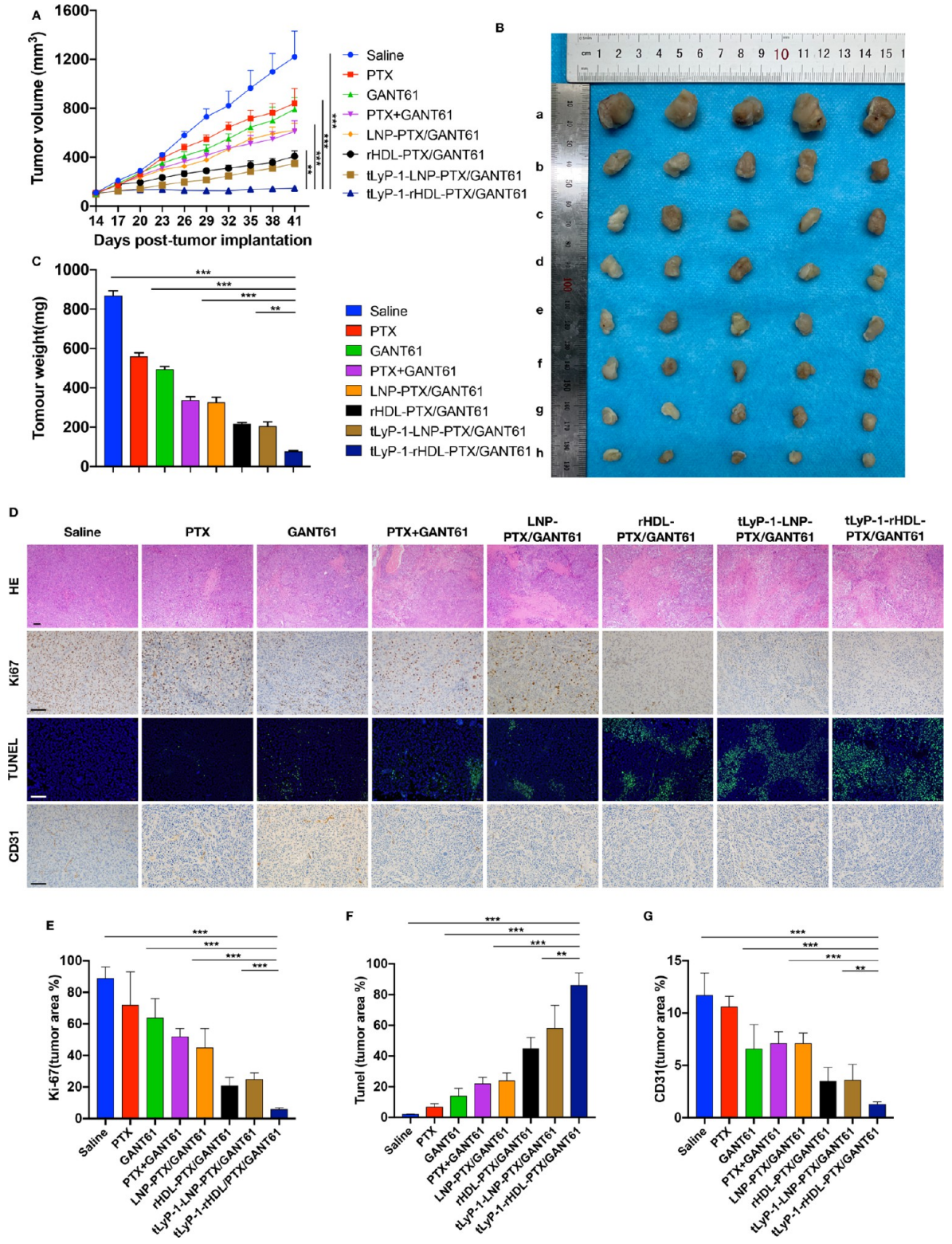

Figure 8. Suppression of *in vivo* tumor growth. (A) Growth of MDA-MB-231 tumors was monitored over time in NCG mice administered the indicated formulations. The GANT1 and PTX levels in each formulation were equivalent. (B,C) Representative images and weights of tumors isolated from the indicated treatment groups. (a) Saline, (b) PTX, (c) GANT61, (d) PTX + GANT61, (e) LNP-PTX/GANT61, (f) rHDL-PTX/GANT61, (g) tLyP-1-LNP-PTX/GANT61, and (h) tLyP-1-rHDL-PTX/GANT61. (D) Tumor sections were stained with H&E, Ki67, TUNEL, and CD31 for histological analyses. Scale bar: 100 μm. (E–G) Quantitative analysis of Ki67, TUNEL, and CD31 staining results (data are means ± S.D., n = 5, *p < 0.05, **p < 0.01, and ***p < 0.001).

231.Luc breast tumor model.[49] Tumor-bearing NCG mice were randomly assigned to undergo treatment with saline, PTX, GANT61, PTX + GANT61, LNP-PTX/GANT61, rHDL-PTX/GANT61, tLyP-1-LNP-PTX/GANT61, or tLyP-1-rHDL-PTX/GANT61 NPs. On day 41 post-tumor implantation, PTX + GANT61 treatment was associated with better

https://doi.org/10.1021/acsami.1c02074
ACS Appl. Mater. Interfaces 2021, 13, 35248–35265

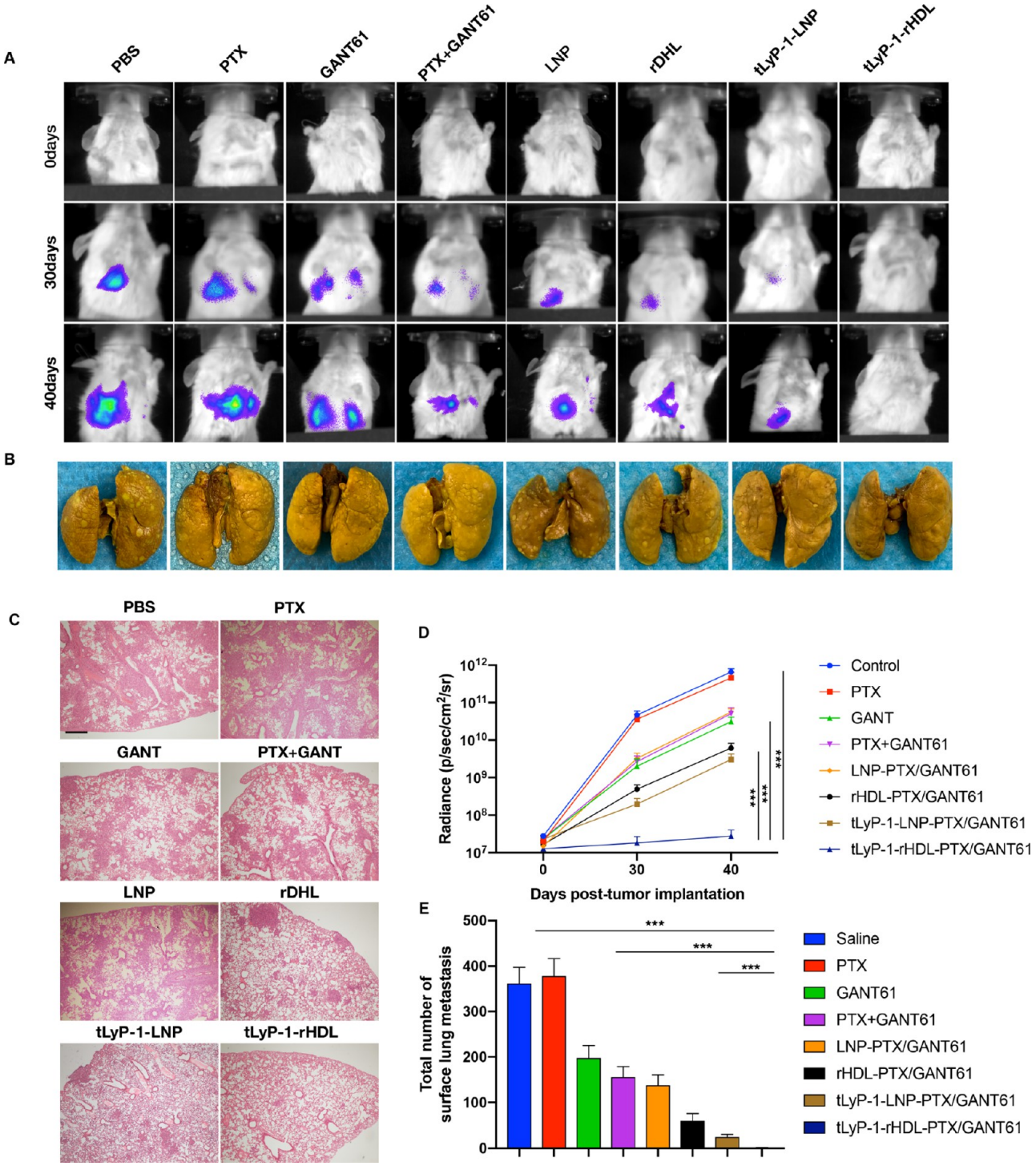

Figure 9. Suppression of *in vivo* tumor metastasis. Bioluminescent signals were imaged (A) and quantified (D) in NCG mice treated with the indicated formulations on days 0, 30, and 40 following tumor implantation. Numbers of metastatic lung modules were (B) imaged and (E) quantified for mice in the indicated treatment groups. (C) Lung tissue sections following H&E staining. All images are representative. Scale bar: 100 μm (data are means ± S.D., n = 5, *p < 0.05,**p < 0.01,and***p < 0.001).

inhibition of tumor growth than was treatment with either of these individual agents. Targeting NPs achieved superior antitumor efficacy compared with drug cocktail solutions or nontargeting NPs, with tumor volumes in mice treated with rHDL-PTX/GANT61 NPs, tLyP-1-LNP-PTX/GANT61, and tLyP-1-rHDL-PTX/GANT61 NPs being approximately 33.8, 28.6, and 12.1% of the values in the saline control group, respectively (Figure 8A,B). The tLyP-1-rHDL-PTX/GANT61 NPs exhibited the greatest antitumor activity, and these findings were confirmed by weighing tumors following the euthanasia of all study animals on day 41 (Figure 8C). These results further illustrated the ability of drug encapsulation in dual-targeting tumor-penetrating NPs to enhance PTX and GANT61 antitumor activity.

Immunohistochemical staining was additionally employed to assess the antitumor efficacy of these NPs. H&E staining

https://doi.org/10.1021/acsami.1c02074
ACS Appl. Mater. Interfaces 2021, 13, 35248−35265

indicated that tLyP-1-rHDL-PTX/GANT61 NP treatment was associated with an increased necrotic area consistent with better therapeutic activity, while Ki-67 staining was reduced following tLyP-1-rHDL-PTX/GANT61 NP treatment relative to all other treatment groups. TUNEL staining was further used to assess tumor cell apoptosis, revealing the highest degree of apoptotic TUNEL staining following the administration of tLyP-1-rHDL-PTX/GANT61 NPs (Figure 8D−F). When CD31 staining was employed as a means of assessing angiogenesis in the different treatment groups, the inhibitory rates in these groups were comparable to the results of tumor inhibition assays (Figure 8D,G).

To test the ability of these NPs to inhibit tumor metastasis *in vivo*, an IVIS imaging system was used to monitor lung metastasis in treated mice. Representative IVIS images and quantitative analyses revealed a time-dependent increase in the burden of such metastases in all mice (Figure 9A). PTX treatment was not associated with any significant decrease in metastasis relative to the control group, whereas GANT61 and PTX + GANT61 treatments were associated with a reduction in metastatic burden, indicating the ability of GANT61 to potently disrupt TNBC metastasis. Consistent with the results of the primary tumor suppression experiments, targeting NPs were better able to suppress lung metastasis relative to free drug solutions. Indeed, a lung bioluminescent signal was almost undetectable following tLyP-1-rHDL-PTX/GANT61 NP treatment (Figure 9D). These results were additionally confirmed through both H&E staining and the counting of surface metastatic nodules in murine lungs in the different treatment groups (Figure 9B,C,E). Together, these data indicated that tLyP-1-rHDL-PTX/GANT61 NPs were able to efficiently inhibit both primary tumor growth and lung metastasis in NCG mice harboring MDA-MB-231 tumors, potentially due to the enhanced intratumoral accumulation of PTX and GANT61 owing to the tumor targeting and penetrating properties of tLyP-1-rHDL NPs. Combined PTX + GANT61 treatment was associated with synergistic antiproliferative activity, suppressing primary tumor growth. GANT61-mediated inhibition of GLI1 also inhibited a number of other downstream regulatory pathways, disrupting TNBC cell malignancy and consequent metastases in tumor-bearing mice. As such, combination PTX + GANT61 treatment mediated *via* tLyP-1-rHDL NP delivery offers promise as a potent therapeutic approach to treat metastatic TNBC.

3.9. Safety Evaluation. It is critical that antitumor therapeutics cause as few adverse side effects as possible, and targeted drug-delivery vehicles may help minimize the risk of such side effects. To assess the systemic toxicity of our different treatment formulations, murine body weight was monitored over time following treatment. While free drug treatments were associated with a significant drop in body weight over time consistent with toxic side effects (Figure S5A), treatment with tLyP-1-rHDL NPs was not associated with any significant weight loss, consistent with the enhanced biocompatibility of these NPs. We additionally evaluated the impacts of these treatments on murine blood cell counts and biochemical parameters. Consistent with the weight loss data, free PTX and GANT61 solutions significantly altered WBC, AST, ALT, and CRE levels relative to control mice (Figure S5B), whereas tLyP-1-rHDL-PTX/GANT61 NP treatment did not significantly alter these parameters, suggesting that these NPs do not disrupt hematological, renal, or hepatic functionality. Histological analyses of major organs from treated mice revealed that all analyzed organs appeared normal and free of any apparent pathology in the tLyP-1-rHDL-PTX/GANT61 treatment group (Figure S5C), consistent with the ability of tLyP-1-rHDL-PTX/GANT61 NPs to efficiently target tumor cells while reducing the risk of adverse systemic side effects *in vivo* in tumor-bearing mice.

4. CONCLUSIONS

In conclusion, we herein successfully developed tLyP-1 peptide-modified rHDL NPs that were able to successfully deliver PTX and GANT61 to tumor cells, thereby facilitating the treatment of metastatic TNBC. The resultant tLyP-1-rHDL-PTX/GANT61 NPs exhibited an appropriate particle size, promising drug loading, and sustained-release properties. Targeting assessments revealed that tLyP-1 peptide and apoA-1 modifications improved the tumor targeting and deep penetration properties of NPs. Overall, these tLyP-1-rHDL-PTX/GANT61 NPs exhibited superior antitumor efficacy relative to free drug preparations. The targeting NPs also amplified the ability of GANT61 to suppress multiple malignant TNBC cellular behaviors associated with tumor metastasis. In a highly metastatic orthotopic breast cancer model, tLyP-1-rHDL-PTX/GANT61 treatment suppressed both primary tumor growth and lung metastasis without inducing obvious adverse systemic toxicity. As such, our dual-targeting tumor-penetrating tLyP-1-rHDL-PTX/GANT61 NPs may represent a promising therapeutic option for the treatment of TNBC.

■ ASSOCIATED CONTENT

Supporting Information

The Supporting Information is available free of charge at https://pubs.acs.org/doi/10.1021/acsami.1c02074.

Expression levels of NRP-1 and SR-B1 in TNBC cells; tumor penetration efficiency of NPs in BT-549 spheroids; prognostic significance of GLI1 gene expression in breast cancer; efficiencies of NPs to inhibited GLI1; efficiencies of NPs to inhibited Vimentin, Snail, and E-cadherin; H&E staining of major organs; and hematology analysis (PDF)

■ AUTHOR INFORMATION

Corresponding Authors

Yuan Guo − *Chongqing Key Laboratory of Ultrasound Molecular Imaging, The Second Affiliated Hospital of Chongqing Medical University, Chongqing 400010, China*; Email: guoyuan77@cqmu.edu.cn

Qiu Zeng − *Department of Vascular Surgery, The First Affiliated Hospital of Chongqing Medical University, Chongqing 400016, China*; orcid.org/0000-0003-0899-3142; Email: zengqiu816@hospital.cqmu.edu.cn

Authors

Chuli Jiang − *Department of Vascular Surgery, The First Affiliated Hospital of Chongqing Medical University, Chongqing 400016, China*

Xingyue Wang − *Chongqing Key Laboratory of Ultrasound Molecular Imaging, The Second Affiliated Hospital of Chongqing Medical University, Chongqing 400010, China*

Biyun Teng − *Department of Vascular Surgery, The First Affiliated Hospital of Chongqing Medical University, Chongqing 400016, China*

Zhe Wang − *Department of Vascular Surgery, The First Affiliated Hospital of Chongqing Medical University, Chongqing 400016, China*
Fenghe Li − *Department of Vascular Surgery, The First Affiliated Hospital of Chongqing Medical University, Chongqing 400016, China*
Yu Zhao − *Department of Vascular Surgery, The First Affiliated Hospital of Chongqing Medical University, Chongqing 400016, China*

Complete contact information is available at: https://pubs.acs.org/10.1021/acsami.1c02074

Author Contributions

The manuscript was written through contributions of all authors. All authors have given approval to the final version of the manuscript.

Notes

The authors declare no competing financial interest.

■ ACKNOWLEDGMENTS

We sincerely acknowledge the financial support by the National Natural Science Youth Foundation of China (no. 81800417).

■ ABBREVIATIONS

APOA-1, apolipoprotein A-1
bFGF, basic fibroblast growth factor
CLSM, confocal laser scanning microscopy
DiI, 1′-dioctadecyl-3,3,3′,3′-tetramethylindocarbocyanine perchlorate
DiR, 1,1′-dioctadecyl-3,3,3′,3′-tetramethylindotricarbocyanine iodide
EPR, enhanced permeability and retention
EGF, epidermal growth factor
GLI1, glioma-associated oncogene transcription factor 1
GEO, gene expression omnibus
HE, hematoxylin & eosin
LNP, liposomal nanoparticle
NP, nanoparticle
NRP-1, neuropilin-1 receptor
PBS, phosphate-buffered saline
PTX, paclitaxel
rHDL, reconstituted high-density lipoprotein
SR-B1, scavenger type B1 receptor
SHH, sonic hedgehog
NPs, nanoparticles
SPC, soybean phosphatidylcholine
TNBC, triple-negative breast cancer
TEM, transmission electron microscopy
TUNEL, terminal deoxynucleotidyl transferase-mediated dUTP-biotin nick end labeling

■ REFERENCES

(1) Heer, E.; Harper, A.; Escandor, N.; Sung, H.; McCormack, V.; Fidler-Benaoudia, M. M. Global Burden and Trends in Premenopausal and Postmenopausal Breast Cancer: A Population-Based Study. *Lancet Glob. Health* **2020**, *8*, e1027−e1037.
(2) Lauby-Secretan, B.; Scoccianti, C.; Loomis, D.; Benbrahim-Tallaa, L.; Bouvard, V.; Bianchini, F.; Straif, K. Breast-Cancer Screening—Viewpoint of the IARC Working Group. *N. Engl. J. Med.* **2015**, *372*, 2353−2358.
(3) Weaver, B. A. How Taxol/Paclitaxel Kills Cancer Cells. *Mol. Biol. Cell* **2014**, *25*, 2677−2681.
(4) Costa, R. B.; Kurra, G.; Greenberg, L.; Geyer, C. E. Efficacy and Cardiac Safety of Adjuvant Trastuzumab-Based Chemotherapy Regimens for HER2-Positive Early Breast Cancer. *Ann. Oncol.* **2010**, *21*, 2153−2160.
(5) Yardley, D. A.; Coleman, R.; Conte, P.; Cortes, J.; Brufsky, A.; Shtivelband, M.; Young, R.; Bengala, C.; Ali, H.; Eakel, J.; Schneeweiss, A.; de la Cruz-Merino, L.; Wilks, S.; O'Shaughnessy, J.; Glück, S.; Li, H.; Miller, J.; Barton, D.; Harbeck, N.; tnAcity investigators. Nab-Paclitaxel plus Carboplatin or Gemcitabine versus Gemcitabine plus Carboplatin as First-Line Treatment of Patients with Triple-Negative Metastatic Breast Cancer: Results from the TnAcity Trial. *Ann. Oncol.* **2018**, *29*, 1763−1770.
(6) Reis-Filho, J. S.; Tutt, A. N. J. Triple Negative Tumours: A Critical Review. *Histopathology* **2008**, *52*, 108−118.
(7) Carey, L. A.; Perou, C. M.; Livasy, C. A.; Dressler, L. G.; Cowan, D.; Conway, K.; Karaca, G.; Troester, M. A.; Tse, C. K.; Edmiston, S.; Deming, S. L.; Geradts, J.; Cheang, M. C. U.; Nielsen, T. O.; Moorman, P. G.; Earp, H. S.; Millikan, R. C. Race, Breast Cancer Subtypes, and Survival in the Carolina Breast Cancer Study. *JAMA, J. Am. Med. Assoc.* **2006**, *295*, 2492−2502.
(8) Steeg, P. S. Targeting Metastasis. *Nat. Rev. Cancer* **2016**, *16*, 201−218.
(9) Riobo-Del Galdo, N.; Lara Montero, Á.; Wertheimer, E. Role of Hedgehog Signaling in Breast Cancer: Pathogenesis and Therapeutics. *Cells* **2019**, *8*, 375−445.
(10) Habib, J. G.; O'Shaughnessy, J. A. The Hedgehog Pathway in Triple-Negative Breast Cancer. *Cancer Med.* **2016**, *5*, 2989−3006.
(11) Ruiz i Altaba, A. Hedgehog Signaling and the Gli Code in Stem Cells, Cancer, and Metastases. *Sci. Signaling* **2011**, *4*, pt9.
(12) Noman, A. S.; Uddin, M.; Rahman, M. Z.; Nayeem, M. J.; Alam, S. S.; Khatun, Z.; Wahiduzzaman, M.; Sultana, A.; Rahman, M. L.; Ali, M. Y.; Barua, D.; Ahmed, I.; Islam, M. S.; Aboussekhra, A.; Yeger, H.; Farhat, W. A.; Islam, S. S. Overexpression of Sonic Hedgehog in the Triple Negative Breast Cancer: Clinicopathological Characteristics of High Burden Breast Cancer Patients from Bangladesh. *Sci. Rep.* **2016**, *6*, 1−11.
(13) Di Mauro, C.; Rosa, R.; D'Amato, V.; Ciciola, P.; Servetto, A.; Marciano, R.; Orsini, R. C.; Formisano, L.; De Falco, S.; Cicatiello, V.; Di Bonito, M.; Cantile, M.; Collina, F.; Chambery, A.; Veneziani, B. M.; De Placido, S.; Bianco, R. Hedgehog Signalling Pathway Orchestrates Angiogenesis in Triple-Negative Breast Cancers. *Br. J. Cancer* **2017**, *116*, 1425−1435.
(14) Benvenuto, M.; Masuelli, L.; De Smaele, E.; Fantini, M.; Mattera, R.; Cucchi, D.; Bonanno, E.; Di Stefano, E.; Frajese, G. V.; Orlandi, A.; Screpanti, I.; Gulino, A.; Modesti, A.; Bei, R. In Vitro and in Vivo Inhibition of Breast Cancer Cell Growth by Targeting the Hedgehog/GLI Pathway with SMO (GDC-0449) or GLI (GANT-61) Inhibitors. *Oncotarget* **2016**, *7*, 9250−9270.
(15) Borah, A.; Pillai, S. C.; Rochani, A. K.; Palaninathan, V.; Nakajima, Y.; Maekawa, T.; Kumar, D. S. GANT61 and Curcumin-Loaded PLGA Nanoparticles for GLI1 and PI3K/Akt-Mediated Inhibition in Breast Adenocarcinoma. *Nanotechnology* **2020**, *31*, 185102−185150.
(16) Calcaterra, A.; Iovine, V.; Botta, B.; Quaglio, D.; D'Acquarica, I.; Ciogli, A.; Iazzetti, A.; Alfonsi, R.; Lospinoso Severini, L.; Infante, P.; Di Marcotullio, L.; Mori, M.; Ghirga, F. Chemical, Computational and Functional Insights into the Chemical Stability of the Hedgehog Pathway Inhibitor GANT61. *J. Enzyme Inhib. Med. Chem.* **2018**, *33*, 349−358.
(17) Isakoff, S. J. Triple-Negative Breast Cancer: Role of Specific Chemotherapy Agents. *Cancer J.* **2010**, *16*, 53−61.
(18) Marupudi, N. I.; Han, J. E.; Li, K. W.; Renard, V. M.; Tyler, B. M.; Brem, H. Paclitaxel: A Review of Adverse Toxicities and Novel Delivery Strategies. *Expert Opin. Drug Saf.* **2007**, *6*, 609−621.
(19) Loprinzi, C. L.; Reeves, B. N.; Dakhil, S. R.; Sloan, J. A.; Wolf, S. L.; Burger, K. N.; Kamal, A.; Le-Lindqwister, N. A.; Soori, G. S.; Jaslowski, A. J.; Novotny, P. J.; Lachance, D. H. Natural History of Paclitaxel-Associated Acute Pain Syndrome: Prospective Cohort Study NCCTG N08C1. *J. Clin. Oncol.* **2011**, *29*, 1472−1478.

(20) Chariou, P. L.; Ortega-Rivera, O. A.; Steinmetz, N. F. Nanocarriers for the Delivery of Medical, Veterinary, and Agricultural Active Ingredients. *ACS Nano* **2020**, *14*, 2678−2701.
(21) Filipczak, N.; Pan, J.; Yalamarty, S. S. K.; Torchilin, V. P. Recent Advancements in Liposome Technology. *Adv. Drug Delivery Rev.* **2020**, *156*, 4−22.
(22) Ali, E. S.; Sharker, S. M.; Islam, M. T.; Khan, I. N.; Shaw, S.; Rahman, M. A.; Uddin, S. J.; Shill, M. C.; Rehman, S.; Das, N.; Ahmad, S.; Shilpi, J. A.; Tripathi, S.; Mishra, S. K.; Mubarak, M. S. Targeting Cancer Cells with Nanotherapeutics and Nanodiagnostics: Current Status and Future Perspectives. *Semin. Cancer Biol.* **2021**, *69*, 52−68.
(23) Zhang, Z.; Chen, J.; Ding, L.; Jin, H.; Lovell, J. F.; Corbin, I. R.; Cao, W.; Lo, P. C.; Yang, M.; Tsao, M. S.; Luo, Q.; Zheng, G. HDL-Mimicking Peptide-Lipid Nanoparticles with Improved Tumor Targeting. *Small* **2010**, *6*, 430−437.
(24) Huang, J.-L.; Jiang, G.; Song, Q.-X.; Gu, X.; Hu, M.; Wang, X.-L.; Song, H.-H.; Chen, L.-P.; Lin, Y.-Y.; Jiang, D.; Chen, J.; Feng, J.-F.; Qiu, Y.-M.; Jiang, J.-Y.; Jiang, X.-G.; Chen, H.-Z.; Gao, X.-L. Lipoprotein-Biomimetic Nanostructure Enables Efficient Targeting Delivery of SiRNA to Ras-Activated Glioblastoma Cells via Macropinocytosis. *Nat. Commun.* **2017**, *8*, 1−18.
(25) Li, M.; Su, Y.; Zhang, F.; Chen, K.; Xu, X.; Xu, L.; Zhou, J.; Wang, W. A Dual-Targeting Reconstituted High Density Lipoprotein Leveraging the Synergy of Sorafenib and AntimiRNA21 for Enhanced Hepatocellular Carcinoma Therapy. *Acta Biomater.* **2018**, *75*, 413−426.
(26) Rui, M.; Xin, Y.; Li, R.; Ge, Y.; Feng, C.; Xu, X. Targeted Biomimetic Nanoparticles for Synergistic Combination Chemotherapy of Paclitaxel and Doxorubicin. *Mol. Pharm.* **2016**, *14*, 107−123.
(27) Raut, S.; Mooberry, L.; Sabnis, N.; Garud, A.; Dossou, A. S.; Lacko, A. Reconstituted HDL: Drug Delivery Platform for Overcoming Biological Barriers to Cancer Therapy. *Front. Pharmacol.* **2018**, *9*, 1154.
(28) Mei, Y.; Tang, L.; Xiao, Q.; Zhang, Z.; Zhang, Z.; Zang, J.; Zhou, J.; Wang, Y.; Wang, W.; Ren, M. Reconstituted High Density Lipoprotein (RHDL), a Versatile Drug Delivery Nanoplatform for Tumor Targeted Therapy. *J. Mater. Chem. B* **2021**, *9*, 612−633.
(29) Delk, S. C.; Chattopadhyay, A.; Escola-Gil, J. C.; Fogelman, A. M.; Reddy, S. T. Apolipoprotein Mimetics in Cancer. *Semin. Cancer Biol.* **2021**, *73*, 158−168.
(30) Samadi, S.; Ghayour-Mobarhan, M.; Mohammadpour, A.; Farjami, Z.; Tabadkani, M.; Hosseinnia, M.; Miri, M.; Heydari-Majd, M.; Mehramiz, M.; Rezayi, M.; Ferns, G. A.; Avan, A. High-Density Lipoprotein Functionality and Breast Cancer: A Potential Therapeutic Target. *J. Cell. Biochem.* **2018**, *120*, 5756−5765.
(31) Somasundar, A.; Sen, A. Chemically Propelled Nano and Micromotors in the Body: Quo Vadis? *Small* **2021**, *17*, 2007102.
(32) Yang, S.; Chen, C.; Qiu, Y.; Xu, C.; Yao, J. Paying Attention to Tumor Blood Vessels: Cancer Phototherapy Assisted with Nano Delivery Strategies. *Biomaterials* **2021**, *268*, 120562.
(33) Rodriguez-Quijada, C.; de Puig, H.; Sánchez-Purrà, M.; Yelleswarapu, C.; Evans, J. J.; Celli, J. P.; Hamad-Schifferli, K. Protease Degradation of Protein Coronas and Its Impact on Cancer Cells and Drug Payload Release. *ACS Appl. Mater. Interfaces* **2019**, *11*, 14588−14596.
(34) Aubin-Tam, M.-E.; Hamad-Schifferli, K. Structure and Function of Nanoparticle−Protein Conjugates. *Biomed. Mater.* **2008**, *3*, 034001.
(35) Hamad-Schifferli, K. Exploiting the Novel Properties of Protein Coronas: Emerging Applications in Nanomedicine. *Nanomedicine* **2015**, *10*, 1663−1674.
(36) Dumond, A.; Pagès, G. Neuropilins, as Relevant Oncology Target: Their Role in the Tumoral Microenvironment. *Front. Cell Dev. Biol.* **2020**, *8*, 662.
(37) Albrecht, C.; Appert-Collin, A.; Bagnard, D.; Blaise, S.; Romier-Crouzet, B.; Efremov, R. G.; Sartelet, H.; Duca, L.; Maurice, P.; Bennasroune, A. Transmembrane Peptides as Inhibitors of Protein-Protein Interactions: An Efficient Strategy to Target Cancer Cells? *Front. Oncol.* **2020**, *10*, 519.
(38) Ruoslahti, E. Peptides as Targeting Elements and Tissue Penetration Devices for Nanoparticles. *Adv. Mater.* **2012**, *24*, 3747−3756.
(39) Roth, L.; Agemy, L.; Kotamraju, V. R.; Braun, G.; Teesalu, T.; Sugahara, K. N.; Hamzah, J.; Ruoslahti, E. Transtumoral Targeting Enabled by a Novel Neuropilin-Binding Peptide. *Oncogene* **2012**, *31*, 3754−3763.
(40) Zhao, H.; Wu, M.; Zhu, L.; Tian, Y.; Wu, M.; Li, Y.; Deng, L.; Jiang, W.; Shen, W.; Wang, Z.; Mei, Z.; Li, P.; Ran, H.; Zhou, Z.; Ren, J. Cell-Penetrating Peptide-Modified Targeted Drug-Loaded Phase-Transformation Lipid Nanoparticles Combined with Low-Intensity Focused Ultrasound for Precision Theranostics against Hepatocellular Carcinoma. *Theranostics* **2018**, *8*, 1892−1910.
(41) Zhu, L.; Zhao, H.; Zhou, Z.; Xia, Y.; Wang, Z.; Ran, H.; Li, P.; Ren, J. Peptide-Functionalized Phase-Transformation Nanoparticles for Low Intensity Focused Ultrasound-Assisted Tumor Imaging and Therapy. *Nano Lett.* **2018**, *18*, 1831−1841.
(42) Hirschhaeuser, F.; Menne, H.; Dittfeld, C.; West, J.; Mueller-Klieser, W.; Kunz-Schughart, L. A. Multicellular Tumor Spheroids: An Underestimated Tool Is Catching up Again. *J. Biotechnol.* **2010**, *148*, 3−15.
(43) Markovitz-Bishitz, Y.; Tauber, Y.; Afrimzon, E.; Zurgil, N.; Sobolev, M.; Shafran, Y.; Deutsch, A.; Howitz, S.; Deutsch, M. A Polymer Microstructure Array for the Formation, Culturing, and High Throughput Drug Screening of Breast Cancer Spheroids. *Biomaterials* **2010**, *31*, 8436−8444.
(44) Wang, R.; Zhao, Z.; Han, Y.; Hu, S.; Opoku-Damoah, Y.; Zhou, J.; Yin, L.; Ding, Y. Natural Particulates Inspired Specific-Targeted Codelivery of SiRNA and Paclitaxel for Collaborative Antitumor Therapy. *Mol. Pharm.* **2017**, *14*, 2999−3012.
(45) Ding, Y.; Wang, Y.; Opoku-Damoah, Y.; Wang, C.; Shen, L.; Yin, L.; Zhou, J. Dual-Functional Bio-Derived Nanoparticulates for Apoptotic Antitumor Therapy. *Biomaterials* **2015**, *72*, 90−103.
(46) Hu, K.; Zhou, H.; Liu, Y.; Liu, Z.; Liu, J.; Tang, J.; Li, J.; Zhang, J.; Sheng, W.; Zhao, Y.; Wu, Y.; Chen, C. Hyaluronic Acid Functional Amphipathic and Redox-Responsive Polymer Particles for the Co-Delivery of Doxorubicin and Cyclopamine to Eradicate Breast Cancer Cells and Cancer Stem Cells. *Nanoscale* **2015**, *7*, 8607−8618.
(47) Lazzari, G.; Couvreur, P.; Mura, S. Multicellular Tumor Spheroids: A Relevant 3D Model for the in Vitro Preclinical Investigation of Polymer Nanomedicines. *Polym. Chem.* **2017**, *8*, 4947−4969.
(48) Győrffy, B.; Lanczky, A.; Eklund, A. C.; Denkert, C.; Budczies, J.; Li, Q.; Szallasi, Z. An Online Survival Analysis Tool to Rapidly Assess the Effect of 22,277 Genes on Breast Cancer Prognosis Using Microarray Data of 1,809 Patients. *Breast Cancer Res. Treat.* **2010**, *123*, 725−731.
(49) Wang, Y.; Xie, Y.; Kilchrist, K. V.; Duvall, C. L.; Oupický, D. Endosomolytic and Tumor-Penetrating Mesoporous Silica Nanoparticles for SiRNA/MiRNA Combination Cancer Therapy. *ACS Appl. Mater. Interfaces* **2020**, *12*, 4308−4322.
(50) Arvizo, R. R.; Miranda, O. R.; Moyano, D. F.; Walden, C. A.; Giri, K.; Bhattacharya, R.; Robertson, J. D.; Rotello, V. M.; Reid, J. M.; Mukherjee, P. Modulating Pharmacokinetics, Tumor Uptake and Biodistribution by Engineered Nanoparticles. *PLoS One* **2011**, *6*, No. e24374.
(51) Simberg, D.; Park, J.-H.; Karmali, P. P.; Zhang, W.-M.; Merkulov, S.; McCrae, K.; Bhatia, S. N.; Sailor, M.; Ruoslahti, E. Differential Proteomics Analysis of the Surface Heterogeneity of Dextran Iron Oxide Nanoparticles and the Implications for Their in Vivo Clearance. *Biomaterials* **2009**, *30*, 3926−3933.
(52) Gupta, A.; Sharma, R.; Kuche, K.; Jain, S. Exploring the Therapeutic Potential of the Bioinspired Reconstituted High Density Lipoprotein Nanostructures. *Int. J. Pharm.* **2021**, *596*, 120272.
(53) Fukuda, M.; Nakano, M.; Miyazaki, M.; Tanaka, M.; Saito, H.; Kobayashi, S.; Ueno, M.; Handa, T. Conformational Change of Apolipoprotein A-I and HDL Formation from Model Membranes

under Intracellular Acidic Conditions. *J. Lipid Res.* **2008**, *49*, 2419−2426.
(54) Ramella, N. A.; Rimoldi, O. J.; Prieto, E. D.; Schinella, G. R.; Sanchez, S. A.; Jaureguiberry, M. S.; Vela, M. E.; Ferreira, S. T.; Tricerri, M. A. Human Apolipoprotein A-I-Derived Amyloid: Its Association with Atherosclerosis. *PLoS One* **2011**, *6*, No. e22532.
(55) Nguyen, S. D.; Öörni, K.; Lee-Rueckert, M.; Pihlajamaa, T.; Metso, J.; Jauhiainen, M.; Kovanen, P. T. Spontaneous Remodeling of HDL Particles at Acidic PH Enhances Their Capacity to Induce Cholesterol Efflux from Human Macrophage Foam Cells. *J. Lipid Res.* **2012**, *53*, 2115−2125.
(56) Vaupel, P. Tumor Microenvironmental Physiology and Its Implications for Radiation Oncology. *Semin. Radiat. Oncol.* **2004**, *14*, 198−206.
(57) Estrella, V.; Chen, T.; Lloyd, M.; Wojtkowiak, J.; Cornnell, H. H.; Ibrahim-Hashim, A.; Bailey, K.; Balagurunathan, Y.; Rothberg, J. M.; Sloane, B. F.; Johnson, J.; Gatenby, R. A.; Gillies, R. J. Acidity Generated by the Tumor Microenvironment Drives Local Invasion. *Cancer Res.* **2013**, *73*, 1524−1535.
(58) Nichols, J. W.; Bae, Y. H. EPR: Evidence and Fallacy. *J. Controlled Release* **2014**, *190*, 451−464.
(59) Gaio, E.; Conte, C.; Esposito, D.; Reddi, E.; Quaglia, F.; Moret, F. CD44 Targeting Mediated by Polymeric Nanoparticles and Combination of Chlorine TPCS(2a)-PDT and Docetaxel-Chemotherapy for Efficient Killing of Breast Differentiated and Stem Cancer Cells In Vitro. *Cancers* **2020**, *12*, 278.
(60) Cui, L.; Wang, Y.; Liang, M.; Chu, X.; Fu, S.; Gao, C.; Liu, Q.; Gong, W.; Yang, M.; Li, Z.; Yu, L.; Yang, C.; Su, Z.; Xie, X.; Yang, Y.; Gao, C. Dual-Modified Natural High Density Lipoprotein Particles for Systemic Glioma-Targeting Drug Delivery. *Drug Delivery* **2018**, *25*, 1865−1876.
(61) Koike, Y.; Ohta, Y.; Saitoh, W.; Yamashita, T.; Kanomata, N.; Moriya, T.; Kurebayashi, J. Anti-Cell Growth and Anti-Cancer Stem Cell Activities of the Non-Canonical Hedgehog Inhibitor GANT61 in Triple-Negative Breast Cancer Cells. *Breast Cancer* **2017**, *24*, 683−693.

https://doi.org/10.1021/acsami.1c02074
ACS Appl. Mater. Interfaces 2021, 13, 35248−35265